THESIS

THE RELATIONSHIP BETWEEN DEEP ROOTS AND THE HYDROLOGIC CYCLE IN THE AMAZON RAINFOREST

Submitted by

Anna Biagi Harper

Department of Atmospheric Sciences

In partial fulfillment of the requirements

For the Degree of Master of Science

Colorado State University

Fort Collins, Colorado

Fall 2008

COLORADO STATE UNIVERSITY

August 4, 2008

WE HEREBY RECOMMEND THAT THE THESIS PREPARED UNDER OUR SUPERVISION BY ANNA BIAGI HARPER ENTITLED THE RELATIONSHIP BETWEEN DEEP ROOTS AND THE HYDROLOGIC CYCLE IN THE AMAZON RAINFOREST BE ACCEPTED AS FULFILLING IN PART REQUIREMENTS FOR THE DEGREE OF MASTER OF SCIENCE

Committee on Graduate Work

_____

Advisor: A. Scott Denning

_____

David Randall

_____

Brian Jones

_____

Department Head: Richard Johnson

ABSTRACT OF THESIS

THE RELATIONSHIP BETWEEN DEEP ROOTS AND THE HYDROLOGIC CYCLE IN THE AMAZON RAINFOREST

Approximately half of the Amazon's evergreen forests are subjected to dry seasons of at least three months. In some regions, there is very little rainfall for up to six months, and yet the forest seems to thrive during the dry, sunny months. Observations show that trees in the Amazon are able to access deep soil moisture by using tap roots with depths of 11 meters or more. Plants also utilize hydraulic redistribution, a process through which water moves through the roots along the water potential gradient.

In order to simulate these essential properties, we made the following modifications in the Simple Biosphere (SiB) model, version 3. First, we increased the soil depth from 3.5 to 10 meters. Second, we implemented an apparent root fraction that takes into account each layer's moisture content, allowing plants to access water in any layer, as long as roots are present. The apparent root fraction is used for determining soil moisture stress and from which layers transpired water is withdrawn. Third, we modified the calculation of soil moisture stress to include a more gradual response to soil moisture deficit. The new version of SiB (called SiB3 PAW for plant available water) was first tested in a single column model (SCM) of the CSU general circulation model (GCM),

BUGS5, and compared results to observations at a tower in the central Amazon forest. Then we ran SiB3 in a full GCM to investigate the feedbacks between surface fluxes and large-scale circulation and regional climate.

In the SCM, SiB3 PAW produces more realistic seasonal cycles of latent and sensible heat flux. Sustained dry season evapotranspiration creates a cooler, more moist boundary layer. The hydrologic cycle is more active, and seasonal and diurnal cycles of the hydrologic cycle are improved.

In the GCM, basin-wide reductions in soil moisture stress result in increased evapotranspiration, precipitation, and moisture recycling in the Amazon basin. In the savannah region of southeastern Brazil, SiB3 PAW produces decreased precipitation and weaker moisture flux, which is more in-line with observations. The improved simulation of precipitation and evaporation also produces a more realistic Bolivian high and Nordeste low. Finally, the changes in tropical forest root zone dynamics are shown to have affects on global moisture convergence, evaporation, sensible heat flux, precipitation, and PBL depth.

Anna Biagi Harper
Atmospheric Sciences Department
Colorado State University
Fort Collins, CO 80523
Fall 2008

ACKNOWLEDGEMENTS

I would like to thank my advisor, Scott Denning, for his support and guidance. His enthusiasm for my work and for science in general has encouraged me many times over the course of my graduate career. I would also like to thank members of my research group and a handful of the members of Dave Randall's group. In particular, thanks to Ian Baker, Mark Branson, and Don Dazlich. Ian has provided an enormous amount of support with SiB and general knowledge of the Amazon. Mark has been extremely helpful with the SCM, and Don has been an invaluable resource for the GCM. I am indebted as well to the many people who have helped me with computational issues - Warren Turkal, Matt Bishop, Ammon Redman, and Kelley Whittmeyer. Finally, thank you to Amy Dykstra and Connie Hale for helping me with my organization and administrative needs.

I also want to thank my family, especially my husband, Chris, for making me laugh and being my support team through the past three years. Thank you to my mom, Pat Lamb, for her encouragement and friendship. Thanks to my friends for keeping life enjoyable and helping me to keep perspective.

My Masters work has depended strongly on data collected during the LBA-ECO field campaign and I would like to thank all of the researchers and data collectors, particularly those involved with the KM83 tower in the Tapajos National Forest.

This work has been supported by the National Science Foundation Science and Technology Center for Multi-Scale Modeling of Atmospheric Processes, managed by Colorado State University under cooperative agreement No. ATM-0425247.

TABLE OF CONTENTS

I. Introduction

The Amazon region is a land of extremes. On one hand, some parts of the river basin receive 3.5 meters of rainfall each year. On the other hand, the dry season can last anywhere from three to six months. Despite these differences in precipitation, observed forest productivity is often greater during the dry season. The reason is increased incoming solar radiation and the ability of the forest to access deep soil moisture.

Therefore, even though the Amazon rainforest is an impressive sight, what allows it to function as it does is not visible from above the ground. Tap roots in the Amazon have been observed to depths of 11 meters. Also, both shallow and deep roots have the ability to move water up and down potential gradients - replenishing deep soil stores during rainy periods and supplying the canopy with moisture during dry periods. These adaptations of the rainforest allow for increased evapotranspiration (Jipp et al. 1998; Nepstad et al. 1994), increased carbon assimilation and forest productivity (Huete et al. 2006) during the dry season.

Many climate models predict an El Nino-like warming of the eastern equatorial Pacific Ocean in the next 50 years (e.g. Cox et al. 2004). During El Nino years, subsidence occurs over tropical South America, resulting in reduced precipitation. Although the Amazon rainforest is well-adapted for seasonal drought, such conditions will test its ability to survive periods of extended drought. Therefore, drought stress in the Amazon has been the focus of numerous observational and modeling studies in recent

year. These studies are summarized in the following papers, but will be briefly introduced here.

In order to study the effects of multi-year drought, one group excluded 35 to 41% of annual rainfall from a 1 ha plot in the Amazon. They initially observed only limited stress on the vegetation, but by the end of the five year study 9% of the trees in the plot had died, total wood production was decreased by more than 60% and above-ground net primary productivity was decreased by approximately 40% (Brando et al. 2008; Nepstad et al. 2004).

Coupled climate/carbon models are useful tools for examining feedbacks between climate and vegetation. In one such model, precipitation decreased in northern Brazil due to a doubling of atmospheric carbon dioxide. This led to limited soil moisture in the Amazon and a transition from forest to savannah by 2050 (Cox et al. 2000, 2004). The precursor to the model used in this study, the simple biosphere model version 2 (SiB2), also predicted a shut-down of the Amazon hydrologic cycle due to inadequate soil moisture under current climate conditions. Clearly, model development and investigation of the mechanisms that trigger these extreme responses are needed.

Modeled drought stress in the Amazon usually is related to inadequate soil moisture. The goal of this work is to investigate the effect of forest root functioning on the Amazonian hydrologic cycle. We do this by testing two representations of soil moisture stress and root distributions in SiB coupled to a general circulation model (GCM). In the end, we aim to make some conclusions about the role of land-atmosphere interactions in the Amazon in exacerbating or mediating extreme drought. This thesis is

divided into two separate papers - one focusing on local fluxes of heat and moisture, and one focusing on large-scale interactions between the vegetation and climate.

First, we completed a three-year run of SiB3 coupled to a single column model (SCM) of a GCM. The SCM cuts the computational cost of coupled model development. It is driven by observations and the modeled atmospheric profile is relaxed toward the observations. This prevents the model from producing an unrealistic atmosphere and allows us to test changes in SiB with relatively few complications. The first part of this thesis presents results from the SCM and examines the simulated fluxes of latent and sensible heat, the hydrologic cycle, and wet season characteristics at a site in the Tapajos National Forest in Brazil.

The next step was to run SiB3 in a fully global GCM, BUGS5. By allowing the vegetation in the coupled model to access deep soil moisture in a realistic manner, we expect to see decreased soil moisture stress and increased dry season evapotranspiration, which is consistent with the observations. The changes in surface fluxes in the GCM should have interesting and important effects on local, regional, and global climate. These results are discussed in the second part of the thesis.

II. PART ONE:

The effect of soil moisture on dry season evapotranspiration and the hydrologic cycle in the Amazon rainforest

Chapter 1. Introduction

The Amazon rainforest is a tremendous resource of ecologic diversity and contains 10 to 15% of the world's total biomass (Houghton et al. 2001). Despite being a very moist region, approximately half of the Amazon's evergreen forests are subjected to dry seasons of at least three months. In some regions, there is very little rainfall for up to six months, and yet the forest seems to thrive during the dry, sunny months. For example, recent satellite data suggests that the forest "greens-up" during the dry season due to the increased solar radiation (Huete et al. 2006).

Understanding the mechanisms that enable the forest to live through extended dry periods is of particular importance considering that the effects of both global warming and land use change are predicted to cause a drier climate in this region (Oliveira et al. 2005). Also, some coupled carbon-climate models predict strong drought stress in the Amazon in the 21st century. The most striking results were from Cox et al. (2000, 2004), whose models predicted a transition from forest to savannah throughout the entire Amazon. The "Amazon dieback" was generally due to a warming and drying of the region, related to a warming pattern over the Pacific. The pattern, which included greater warming over the Eastern Pacific, resembled conditions during El Nino, when rainfall is typically reduced in northern Brazil (Cox et al. 2004). Other carbon/climate models also

predict drought stress in the Amazon (Friedlingstein et al. 2001; Bala et al. 2005; Liu 2004).

Dry season evapotranspiration (ET) depends on both meteorological and physiological factors, and is closely related to photosynthesis. Decreased cloud cover supplies the canopy with stronger incoming radiation and thus more energy. The solar radiation drives ET through increased stomatal conductance and boundary layer turbulence. Other meteorological conditions like the vapor pressure deficit (VPD) and winds can also affect stomatal conductance and evaporation.

Meanwhile, the roots in the Amazon are well suited for allowing dry season survival. Tap roots have been observed up to 11 m deep (Nepstad et al. 1994; Jipp et al. 1998; Nepstad et al. 2002). Hydraulic redistribution also allows the plants to access water from shallower soil layers, where most of a tree's fine roots are located. Through this process, water moves along the water potential gradient to supply moisture to the canopy when the air is dry. It can also work in the reverse to replenish deep soil water, for example, during a rainfall following a rainless period (Oliveira et al. 2005). Hydraulic redistribution not only increases a plant's drought tolerance, it also enables the plant to maintain transpiration and carbon sequestration during seasonal droughts (Saleska et al. 2003; Oliveira et al. 2005) and has been shown to improve the seasonal cycle of evapotranspiration in land models (Lee et al. 2005).

The efficiency of Amazonian roots has been documented by several studies. At Paragominas in the eastern Amazon from 1991 through 1994, daily dry season rates of ET from primary and secondary growth forest and from pasture exceeded rainfall by a

factor of 2.2, 2.1, and 1.8, respectively (Jipp et al. 1998). A number of other studies in the eastern and central Amazon Basin also found increased ET during the dry season, as well as relatively higher ET in areas with less dry season rainfall (e.g. Nepstad et al. 1994). Other ecological factors affecting dry season ET include the amount of soil water, the plant's ability to extract it, and the shoots' ability to withstand the stress induced as moisture is depleted and soil water potential falls (Jipp et al. 1998).

These studies suggest that sunlight may exert more influence than rainfall on forest transpiration and productivity. During the dry season, assimilation of carbon by the plants is encouraged by the abundance of photosynthetically active radiation (PAR) and the ability of the plants to access deep soil moisture. A satellite-derived quantity, the MODIS Enhanced Vegetation Index (EVI, an index of canopy photosynthetic capacity), measured from 2000 to 2005 across the Amazon Basin, increased by 25% during the dry season in forests. These observations are consistent with measurements of gross primary production (GPP) by two eddy flux towers in the Tapajos National Forest (km 67 and km 77 towers) (Huete et al. 2006).

In order to study the long-term effects of drought, Nepstad and Brando (Nepstad et al. 2002; Brando et al. 2008) excluded water from plots of forest in the Amazon during the rainy seasons of 2000 through 2004 in the Tapajos National Forest. During these four years, wet season rainfall was excluded from a 1 ha plot, resulting in a reduction in rainfall of 35-41%. After the first year, there were relatively low reductions in wood production (13%), leaf area index (LAI), and above-ground net primary productivity (ANPP) (12%). There was also no detectable increase in leaf drought stress (Brando et al. 2008).

However, over the following four years, total wood production and ANPP decreased by up to 63% and 41%, respectively. Other changes were an inhibited formation of new leaves, a decrease in surface (0-2 m) and deep soil (2-11 m) water content, reduced photosynthetic capacity, stem radial growth, fine litterfall, and fruiting (Nepstad et al. 2004). Overall, 9% of the trees on the exclusion plot died over the five-year experiment. In 2005, the first year of recovery, litterfall fully recovered and wood production rebounded to only 13% less than the control plot. Most likely, decreased competition in the plot aided this rapid recovery (Brando et al. 2008).

Therefore, the majority of observational evidence suggests that the Amazon rainforest not only survives short-term dry periods, it also thrives during these times due to a combination of increased radiation and the trees' ability to access soil moisture. This survival mechanism is limited during longer-term droughts, as shown by Nepstad et al. (2007) and Brando et al. (2008). Unfortunately, model results have not reproduced this ability. For example, in the Tapajos National Forest in Brazil, Saleska et al. (2003) showed that two ecosystem models (IBIS and TEM) got the seasonal cycle of net ecosystem exchange exactly wrong. While observations showed net flux of carbon from the forest in the wet season, and net uptake in the dry season, the models showed the opposite cycle.

Another example is the Simple Biosphere Model (SiB; Sellers et al. 1986, Sellers et al. 1996, Baker et al. 2007). SiB has historically had problems simulating fluxes of heat and moisture in the Amazon (Randall et al. 1996, Liu et al. 2004). However, by isolating certain root and soil functions in the model, Baker et al. (2008 – using SiB

version 3.0) were able to obtain more realistic results with regards to carbon fluxes at certain cites in the Amazon.

Implementing an interactive land-surface model such as SiB is now standard procedure for many climate models. In such a role, SiB parameterizes surface sensible and latent heat fluxes, and creates a more realistic boundary layer. Unfortunately, testing SiB in a full global general circulation model (GCM) is not a simple task. The single column model (SCM) is a useful tool for cutting the computational cost of coupled model development (Betts and Miller, 1986; Randall and Cripe, 1999). The SCM contains all of the same code as its global counterpart, but it only applies to a single grid cell, or column. Instead of reading in variables from neighboring grid cells, the SCM is forced by observations. It is often used for evaluating cloud models and other physical parameterizations in a time-efficient manner. A disadvantage of the SCM is that feedbacks involving the large-scale circulation cannot be included. However, an upside of this is that the SCM makes it easier to test parameters or to diagnose problems in the results without complications from the rest of the model (Randall et al. 1992). Therefore, by coupling SiB to an SCM, we can develop and test improved treatments of root zone stress.

In this paper, we will show results from coupling the most recent versions of SiB into a single column of the BUGS GCM. In Section 2, the models, their coupling, driving data and the site are described. In Section 3, results are given for the coupled SCM. Important implications of this study and future work are discussed in Section 4.

2. Methods

2.1 MODEL DESCRIPTIONS

This study utilizes several modeling tools to better understand the Amazon hydrologic cycle, including SiB, a GCM, and a single-column model.

SiB

The Simple Biosphere (SiB) model is based on a land-surface parameterization scheme that computes biophysical exchanges (Sellers et al. 1986) and ecosystem metabolism (Sellers et al. 1996a; Denning et al. 1996). Photosynthetic carbon assimilation is parameterized based on the enzyme kinetics of Farquhar et al. (1980) and is linked to the surface energy budget and atmospheric climate via stomatal conductance (Collatz et al. 1991, 1992; Sellers et al. 1996a; Randall et al. 1996). SiB calculates fluxes of heat, moisture, momentum, and CO_2 from the gradients of each between the canopy air space and the free atmosphere, scaled by a resistance. The equations for sensible and latent heat flux are in Figure 2.1 (adapted from Sellers et al. 1996a).

In this study, four different set-ups of SiB are compared: 1) SiB2.0; 2) a version of SiB3 with soil moisture stress calculated using root-weighted stress (SiB3 RW); 3) SiB3 with deep roots and soil moisture stress calculated using plant available water (SiB3 PAW); and 4) a version of SiB3 PAW with hydraulic redistribution (SiB3 HR).

SiB2.0

SiB2, described by Sellers et al 1996, Randall et al 1996, and Denning et al 1996, consists of three soil layers, reaching 2.5 meters depth. Moisture in the top layer is either stored or evaporated. The middle layer contains all of the roots and is responsible for all of the transpiration. The bottom layer is only used for drainage and recharge.

$$H_t = \frac{(T_a - T_m)\rho c_p}{r_a}$$
$$\lambda E_t = \frac{(e_a - e_m)\rho c_p}{\gamma r_a} \qquad (1)\ \&\ (2)$$

H_t	total sensible heat flux from the canopy air space (CAS) (W m^{-2})
E_t	total evapotranspiration rates from the CAS (kg m^{-2} s^{-1})
T_a, e_a	air temperature, vapor pressure in canopy air space (K, Pa)
T_m, e_m	air temperature, vapor pressure at top of mixing layer (K, Pa)
ρ, c_p	density, specific heat of air (kg m^{-3}, J kg^{-1} K^{-1})
γ	psychrometric constant (Pa K^{-1})
λ	latent heat of vaporization (J kg^{-1})
r_a	aerodynamic resistance between CAS and reference height (s m^{-1})

Figure 2.1: Equations governing sensible and latent heat fluxes in the Simple Biosphere Model.

SiB3.0 using a root-weighted stress calculation (SiB3 RW)

SiB3 includes a 3.5 meter deep, 10 layer soil with a water extraction root profile extending through all layers (Figure 2.2). This change is adapted from the Community Land Model (Dai et al. 2003) and based on the earlier NCAR Land Surface Model

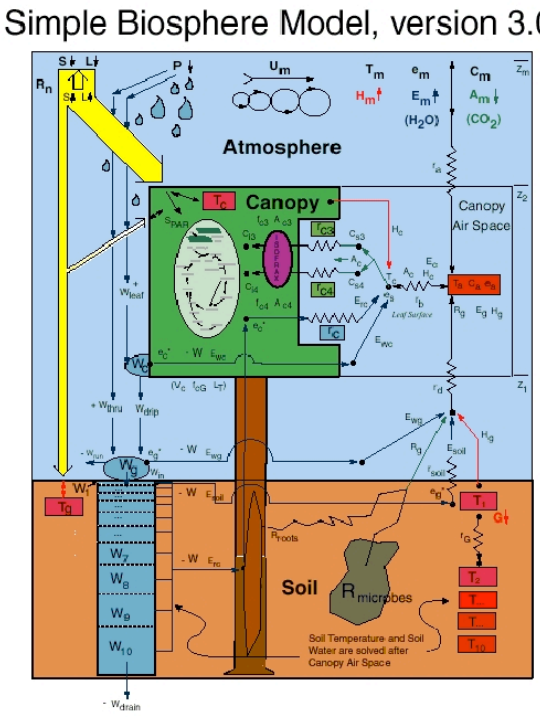

Figure 2.2 SiB 3.0 treatment of heat, moisture, and carbon dioxide fluxes from the ground and the canopy. Terms are defined in Figure 2.1.

(Bonan 1996). Soil moisture stress is calculated layer-by-layer and is weighted by the fractional amount of roots in each layer. In the canopy air space (CAS), temperature, water vapor, CO_2, heat and water fluxes are predicted from time step to time step.

SiB3 using plant available water to calculate stress (SiB3 PAW)

In the following two versions of the model, which are also fully described in Baker et al. (2008), soil depth is increased from 3.5 meters to 10 meters. Also, plant available water (PAW) replaces root-density weighted water to calculate water stress. A third change to the SiB3 PAW simulation is the optimum soil moisture for heterotrophic respiration. We increased the value to 75% of saturation, which is more in line with the observed annual average volumetric soil moisture at 10 cm (Baker et al. 2008).

SiB3 PAW with hydraulic redistribution

Hydraulic redistribution allows water to move along the water potential gradient in roots and has recently been found to be essential to providing water to trees in the

Amazon during dry periods (Oliviera, 2005). Incorporation of hydraulic redistribution into the NCAR Community Land Model led to increased dry season evapotranspiration and decreased temperatures in the Amazon, which affected the global climate (Lee et al. 2005). To simulate this function, we add a hydraulic redistribution term to the calculations of vertical movement of soil water. This allows the roots to move water downwards in times of excess rainfall, and to move the water upwards during dry periods. This version of the model also includes the plant available water calculation of soil moisture stress, deep roots, and revised optimum soil moisture parameter.

BUGS5

BUGS5 is an atmospheric general circulation model that has evolved from the 1980's UCLA GCM. The model uses an explicit planetary boundary layer (PBL) depth with prognostic turbulent kinetic energy. The PBL is the lowest level in the model, which uses a modified sigma coordinate (Suarez et al. 1983; Randall et al. 1985).

The radiation parameterization in the GCM utilizes a 2-stream method for calculating broadband and heating rages in the shortwave and longwave and accounts for IR scattering (Stephens et al. 2001; Gabriel et al. 2001). The cumulus cloud parameterization includes ice phase microphysics, prognostic convective closure, and multiple cloud-base levels (Arakawa and Schubert 1974; Randall and Pan 1993; Pan and Randall 1998; Ding and Randall, 1998). The stratiform cloud parameterizations include prognostic cloud droplets, ice crystals, and hydrometeors (Fowler et al. 1996; Fowler and Randall 2002). BUGS5 uses a dynamical core based on a spherical geodesic grid (Ringler et al. 2000; Randall et al. 2002).

SCM

We performed a series of numerical simulations using a single-column model (SCM) of BUGS5, the Colorado State University (CSU) General Circulation Model (GCM). The SCM comprises the full GCM physics, such as radiation, convection, cloud microphysics, and PBL treatments. Advective tendencies in temperature, water vapor, and other prognostic quantities that would ordinarily be computed using neighboring grid columns are instead prescribed as "forcing" from another source.

In this experiment, we chose to use "relaxation forcing" to prescribe the advective tendencies, as described by Randall and Cripe (1999). In this method, the horizontal advective tendencies of temperature and water vapor are computed by relaxing their profiles toward their observed upstream values, scaled by a relaxation timescale that depends on the time required for the wind to carry parcels across the grid column.

$$\frac{\partial q}{\partial t} = \frac{q_{in} - q}{\tau_{adv}} - \omega \frac{\partial q}{\partial p} + P \qquad (3)$$

$$\frac{1}{\tau_{adv}} = \frac{2V}{d}$$

In Equation 3, q is any scalar variable and P represents the model physics. V is the average wind speed in the region. d is related to the distance across the region and its orientation depends on the wind direction.

The advantage of relaxation forcing is it prevents the model from creating unrealistic atmospheric conditions, which allows physical parameterizations within the GCM to be tested in a realistic atmosphere. Furthermore, because the atmospheric

conditions are forced to be realistic, it is possible to compare results from SiB to surface observations. The use of relaxation forcing will prevent the modeled atmosphere from completely drying out, as occurred in previous versions of BUGS/SiB (Liu 2004). Therefore, the point of the simulations described in this paper is to investigate how SiB allows the canopy to respond to realistic atmospheric conditions. As is shown by offline versions of SiB, latent and sensible heat fluxes have historically been incorrect in the Amazon, and we hope to remedy this problem with the changes described above. A disadvantage of using relaxation forcing in the tropics is the fact that horizontal advective tendencies tend to be weak. Therefore, a small error in the simulated value could contain a large fractional error in the model (Randall and Cripe 1999).

2.2 ROOT-WEIGHTED VERSUS PLANT AVAILABLE WATER STRESS

SiB calculates a potential photosynthetic rate that is dependent on factors such as leaf area, CO2 concentration at the leaf surface, and radiation absorbed by the canopy. Potential photosynthesis is then scaled by three stress factors in order to maximize carbon assimilation while minimizing water loss. Stress can originate from less than optimal temperature, humidity, and soil moisture. This study focuses on the latter.

Figure 2.3 shows treatments of root depth and density in SiB3 RW and SiB3 PAW. SiB3 PAW corresponds to the deep soil SiB3 discussed in Baker et al. (2008). Root depth is 3.5 and 10 meters in SiB3 RW and SiB3 PAW, respectively, allowing the latter version of the model to hold more water in the soil. Furthermore, the removal of transpired water is treated differently. In SiB3 RW, transpired water is removed from the soil based on

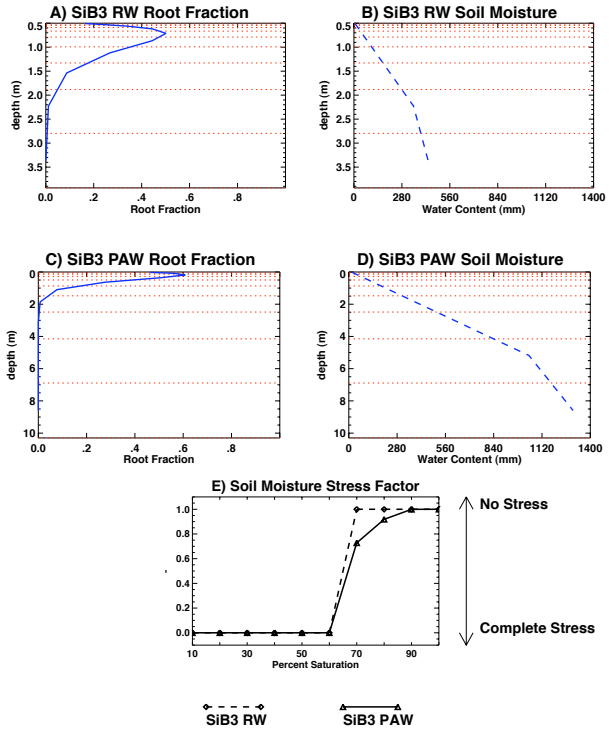

Figure 2.3 Treatments of roots and soil moisture stress within SiB3 RW and SiB3 PAW.

actual root fractions in each layer (Figure 2.3a). While this seems physically realistic, it does not take into account hydraulic redistribution, which is essentially the ability of roots to move water to and from areas of water deficit and surplus (Oliveira et al. 2005). In SiB3 PAW, transpired water is removed from an "apparent" root fraction, which takes into account both actual root fraction (Figure 2.3c) and moisture content (Figure 2.3d) in each layer. As is shown in Figure 2.3 (b & d), the most water resides in the deepest layers. Although root density is low in these layers, it is greater than zero. Therefore, in SiB3 PAW, the vegetation is able to access moisture throughout the rooting profile. This new calculation of soil moisture stress is a function of plant available water within the entire rooting profile, independent of layer-by-layer moisture content or root fraction. The ability of deep roots to access large amounts of water has been observed by Jipp el al. (1998) and Nepstad et al. (1994).

Another key difference between SiB3 RW and SiB3 PAW is the calculation of soil moisture stress (Figure 2.3e). The soil moisture stress factor is calculated so that a value of 1.0 means there is no stress on the vegetation from soil moisture, while a value of 0.0 means the vegetation is completely stressed by lack of soil moisture. In both versions of the model, plants will not transpire when water content is below the wilting point and slight stress is imposed when moisture is below field capacity. Stress slowly increases in SiB3 RW until just above the wilting point, at which point it increases rapidly. Although this response is realistic on a plant-to-plant basis, a smoother response is more realistic on the scale of a grid cell. Therefore, in SiB3 PAW, stress increases more gradually below field capacity.

2.3 DRIVING DATA

The SCM is forced by model-derived variables from NCEP Reanalysis II, available every six hours on a 2.5° x 2.5° grid. Since the footprint of the column is much larger than the footprint of the tower, we should not expect the model to exactly mimic the observations at the Tapajos tower, but we do expect the same seasonal cycles. The variables used were temperature, relative humidity, meridional and zonal wind, surface pressure, and geopotential height.

Modeled fluxes of heat and water vapor are dependent not only on meteorological drivers (temperature, humidity, wind, and precipitation) but are also highly dependent on the characteristics of the canopy vegetation and soil type. SiB3.0 specifies these vegetation and soil parameters as monthly values based on vegetation type. The

parameters were specified using a combination of land cover type (Hansen et al., 2000), monthly maximum normalized difference vegetation index (NDVI) derived from advanced very high-resolution radiometer (AVHRR) data (Tiellet et al., 2000), and soil properties observed in the area (Silver et al., 2000). Time-invariant vegetation biophysical parameters such as canopy height, leaf angle distribution, leaf transmittance, and parameters related to photosynthesis are based on values recorded in the literature and assigned via look-up tables (Sellers et al., 2006b). Time-varying vegetation biophysical parameters such as fraction of photosynthetically active radiation (FPAR), fraction of vegetation cover, greenness fraction, and leaf area index (LAI) are calculated from one year of NDVI monthly maximum value composites for the site. The time-varying parameters are based on the equations in Sellers et al. (1992, 1996b) and Los et al. (2000). Soil hydraulic and thermal parameters are calculated from the percent of sand and clay in the soil using equations from Clapp and Hornberger (1978).

2.4 SITE DESCRIPTION

This study focuses on a flux tower located in the Tapajos National Forest, which was operated from 2001 to 2004 as part of the Large-scale Biosphere-Atmosphere Expriment in Amazonia (LBA), an international research initiative led by Brazil. The tower is located near the km 83 marker on the Santarem-Cuiaba highway (BR 163), approximately 70 km south of Santarem, in the state of Para, Brazil (3.01030°S, 54.58150°W). The site was selectively logged in September 2001 (da Rocha et al., 2004). Data from the tower includes meteorological and flux data. Of particular interest to this

study are half-hourly measurements of air temperature, precipitation, and radiation, as well as fluxes of heat and water vapor. The experimental design and instrumentation are fully described by Goulden et al. (2004) and Miller et al. (2004).

Rainfall in the Amazon is seasonal, with a dry season extending from approximately August through December in the region of the Tapajos tower (Figure 2.4a). At the Tapajos tower, from 2001 to 2003, the average annual rainfall was 1480 mm. The nature of convection creates high spatial variability in the precipitation field. For example, at a tower located 16 km away, the total precipitation for 2002 was 1882 mm (Liu 2004).

The site's dry season length and intensity varied from year to year. For the purpose of this study, we use monthly rainfall of 100 mm (or approximately 3.33 mm/ day) as a threshold for defining dry season months. For clarity, the dry season is marked in seasonal plots by the yellow shading. In 2002 and 2003, some months during the "dry season" had more than 100 mm of rain but are still included in the dry season because the preceding and following months were had less rainfall. In 2001, there was little rainfall from July through December. The following year, almost no rain fell from August to October. The dry season was relatively wet in 2003.

Monthly means of other meteorological variables are compared to NCEP II Reanalysis in Figure 2.4. Because NCEP was used to drive the models, we expect there to be some influence from these variables in the model results. In Figure 2.4, canopy air space and PBL observations are from 10 and 64 meters, respectively. However, the modeled PBL depths are usually on the order of 50 to 80 hPa (see Figure 3.4), which

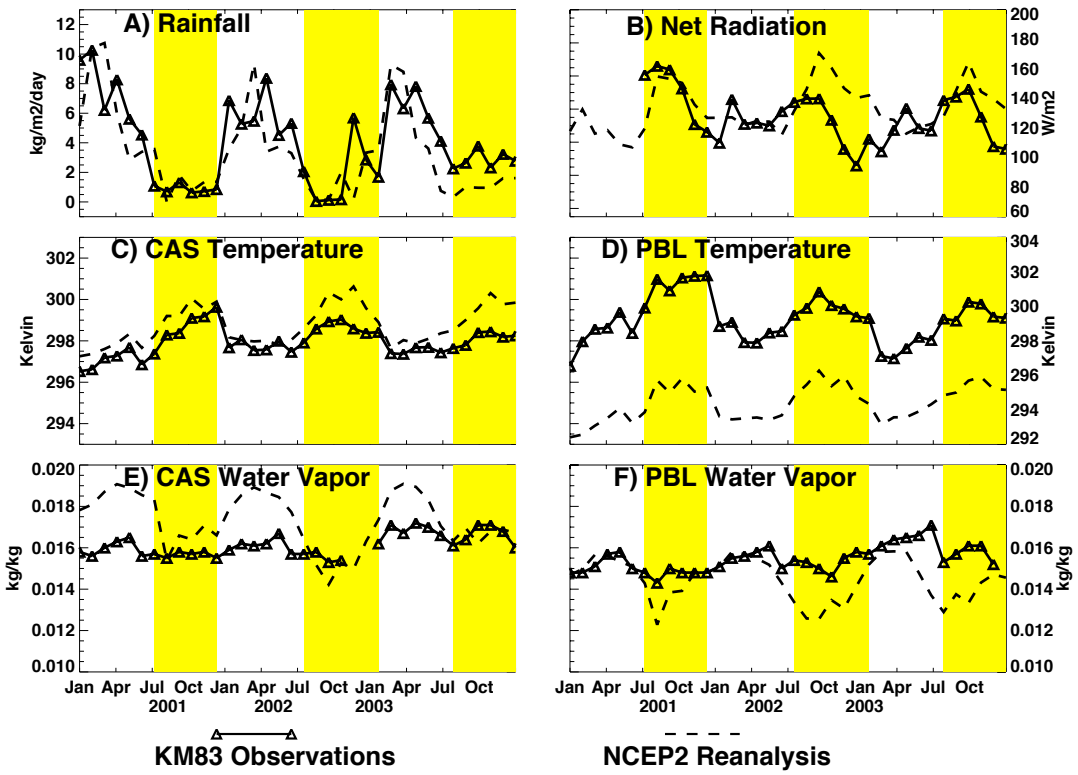

Figure 2.4 Monthly mean values of rainfall (a), net radiation (b), and temperature water vapor for the canopy airspace (c,e) and PBL (d,f). Black triangles represent observations at the KM83 tower in the Tapajos National Forest, Brazil (3S, -55W). The PBL measurements are from 64 m and CAS measurements are from 10 m. The shading represents months with less than 100 mm of rainfall. The dashed line is the NCEP II Reanalysis product, taken from a 2.5x2.5 degree cell centered on 2.5S, -55W. The PBL measurements are from 925 hPa and CAS measurements are from 1000 hPa. The shading represents months with less than 100 mm of rainfall.

typically occurs at less than 1500 m. Therefore, the 64 meter observations are representative of the mixed layer just above the canopy, but are much lower than the middle of the boundary layer. NCEP values for the CAS are taken at 1000 hPa and for the PBL at 925 hPa. Water vapor is not plotted for November and December of 2002, when observed values at 2m and 10m were consistently above 0.025 kg/kg – which is much higher than the rest of the observational record. The longwave components of net radiation were missing from the observations in early 2001.

The seasonality of net radiation has interesting contributions from the longwave and shortwave components, with the latter usually playing a more dominant role. During

the dry season, more sunlight reaches the surface and more longwave radiation is emitted. The net result is increased radiation early in the dry season. As mentioned in the introduction, the increased photosynthetically available radiation also serves to contribute to high dry season stomatal conductance. However, as the season continues, less solar radiation reaches the surface and the downwelling longwave radiation gradually increases. This could be due to gradually increasing cloudiness, or due to the presence of aerosols from dry season forest fires. Either way, the net effect is gradually decreasing radiation until a minimum is reached near the end of the dry season. During the wet season, longwave trapping increases, causing the net radiation to increase as well.

Observed water vapor and temperature both show a larger seasonal cycle above the canopy than within it. This is possibly due to the competing effects of large-scale moisture transport and local ecophysiology. Observations show that latent heat flux continues through the dry season at KM83, which would regulate moisture and heat content throughout the year. Above the canopy, the effects of large-scale atmospheric conditions are more prevalent. Despite the months-long periods with little rainfall, observed sensible and latent heat fluxes show very little variability throughout the seasons (Figure 2.5). In fact, relatively strong fluxes of latent heat occur during the dry seasons, suggesting

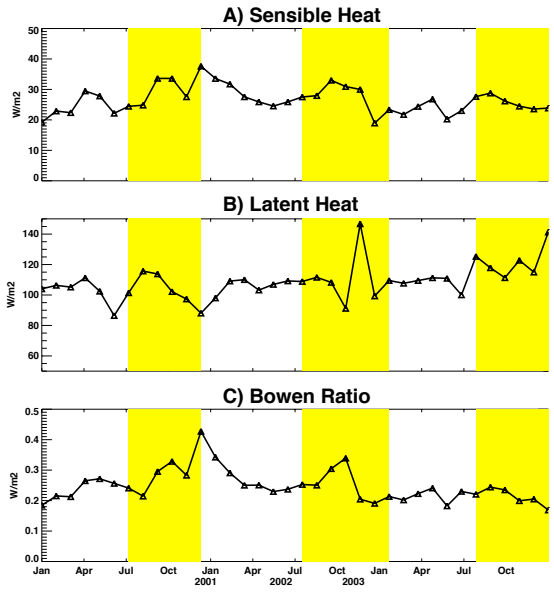

Figure 2.5 Observed fluxes of sensible and latent heat, and the observed Bowen ratio, from the KM83 tower in the Tapajos National Forest.

that the forest has access to a more than adequate supply of moisture. This seasonal cycle is somewhat unexpected, and usually not captured by land surface models. The observed Bowen ratio varies from 0.17 to 0.43. Higher values tend to occur during the dry season, with the exception of 2003, which was a relatively wet dry season.

3. RESULTS

3.1 GENERAL METEOROLOGY

Modeled versus observed rainfall, moisture, temperature, and radiation are shown in Figure 3.1. All versions of the model produce a similar seasonal cycle in rainfall as compared to observations (results from SiB2 and SiB3 HR are not shown in this figure, but are very similar to those from SiB3 RW and SiB3 PAW, respectively). As discussed earlier, the temperature and moisture profiles are relaxed toward the driver data, preventing the model from producing unrealistic atmospheric conditions. Nevertheless,

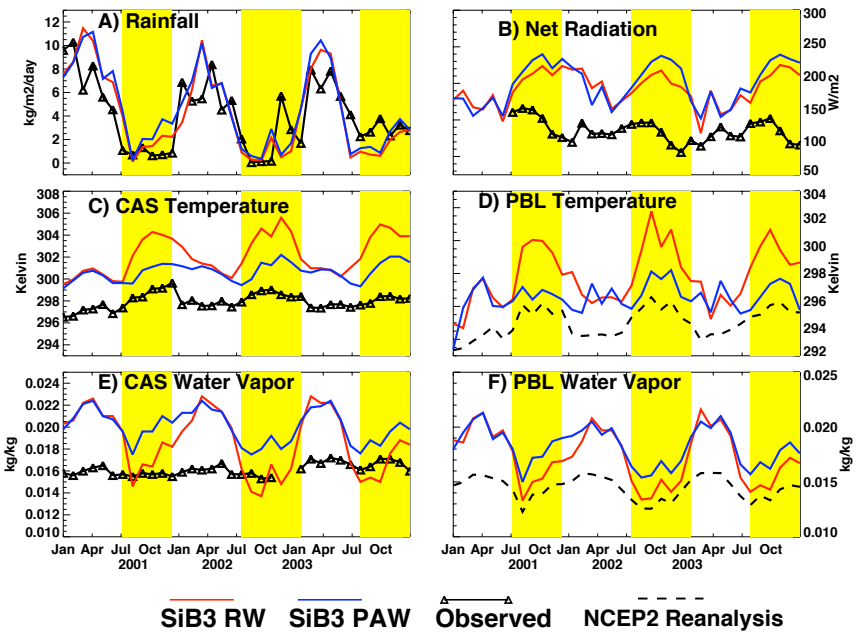

Figure 3.1 Monthly mean values of rainfall (a), net radiation (b), and temperature water vapor for the canopy air space (c,e) and PBL (d,f). Black triangles represent observations at the KM83 tower in the Tapajos National Forest, Brazil. Blue and red lines are model results. Observed values at the KM83 tower at 10m are used for the CAS, and NCEP values from 925 hPa are used for the PBL. The shading represents months with less than 100 mm of rainfall.

the modeled canopy air space (CAS) is too warm and moist, and the modeled PBL is usually too warm and dry. During the dry season, the temperatures are improved in SiB3 PAW, while the water vapor is closer to observations in SiB3 RW.

The seasonal cycle and magnitude of net radiation is much stronger in SiB than in the observations and is investigated further in Figure 3.2. Downwelling longwave is similar between the models and observations (3.2a). Both atmospheric water vapor and aerosols trap and re-emit longwave radiation. The modeled atmosphere near the surface is more moist than the observations, but the model does not include aerosols from biomass burning. Fires are common during the dry season, so it is logical for this to be a large contributor to the radiation differences. It is possible that the competing effects of stronger water vapor and unresolved aerosols nearly cancel each other out to give a close fit between models and observations for downwelling longwave radiation. The stronger upwelling longwave radiation in the models is probably due to a warmer than observed surface (e.g.: Figure 3.1c).

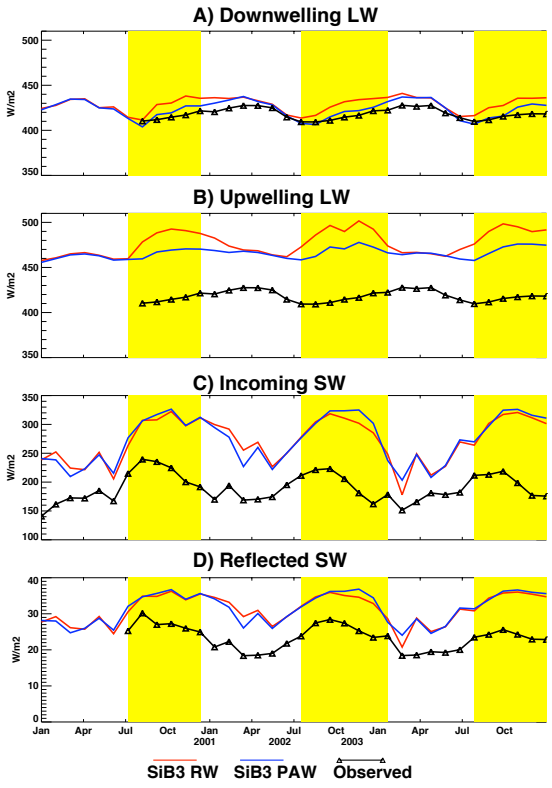

Figure 3.2 Modeled and observed components of the radiation budget.

The largest discrepancies come from the shortwave radiation budget. Incoming solar radiation is often more than 100 W/ m^2 stronger in the models, especially during the dry season (Figure 3.2c). This could be due to underestimated cloud cover

in the model, or to lack of modeled aerosols. In addition, less radiation is being reflected in the models (Figure 3.2d). The observed surface albedo is about 14-15%, while model surface albedo is 11-12%. Because the modeled surface is receiving more radiation, we expect stronger than observed total fluxes of sensible and latent heat. Again, we hope to mimic the seasonal cycles of these fluxes rather than their exact observed values.

3.2 SEASONAL HEAT AND MOISTURE FLUXES

Modeled fluxes of sensible and latent heat flux are compared to tower observations in Figure 3.3. Because of the similarities between SiB2 and SiB3 RW, and between SiB3 PAW and SiB3 HR, future plots will only show the RW and PAW versions. Although the observations show very little seasonality, the seasonal cycles of latent and sensible heat are severely over-amplified in SiB3 RW. These differences are largest during the dry season, when latent heat is too low and sensible heat is too high. The dry season Bowen ratio reaches 5, as compared to an observed ratio of less than 0.43. During the dry seasons of all three years, the vegetation is strongly stressed, especially during the middle of the day. This prevents the plants from being able to transpire, and instead the majority of the radiation they absorb is released via sensible heat.

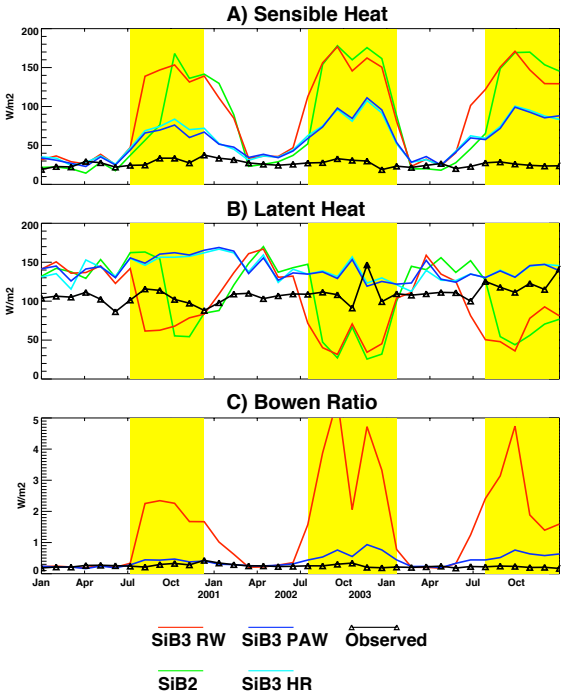

Figure 3.3 Monthly mean sensible and latent heat flux and Bowen ratio.

The seasonal cycle of latent heat is greatly improved with SiB3 PAW (Figure 3.3b). Soil moisture stress still increases during the dry season, but not nearly as much as in the root-weighted case (Figure 3.4a). As a result, plants continue to transpire in the absence of rain, and CAS and PBL specific humidities show weaker seasonal cycles than in SiB3 RW, which is more in line with the observations.

Despite the improvements, the SiB3 PAW latent heat flux is always higher than the observations. This is probably a combination of the overestimated radiation and the fact that the modeled atmosphere is too moist, especially in the rainy seasons. Not only are modeled canopy air space and mixed layer specific humidities higher than observed, but the atmospheric moisture gradient is also too high (Figure 3.4b). However, it is encouraging that the seasonal cycle of latent heat is closer to the observations in the SiB3 PAW model.

The sensible heat flux is closely linked to canopy air space and boundary layer temperature (Figure 3.5). Although the modeled PBL is usually cooler than observed, the CAS is always warmer by at least 1 K. This results in a stronger than observed temperature gradient and the over-calculation of sensible heat fluxes in both versions of the model (Figure 3.5c). In SiB3 RW, the CAS temperature gets almost 10 K warmer than the observed CAS (Figure 3.2c). Due to stomatal

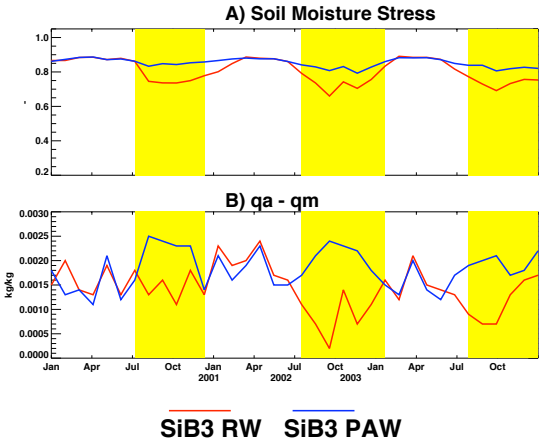

Figure 3.4 Monthly mean values of: A) soil moisture stress factor. A value of 1.0 means the plants are completely unstressed. B) The moisture gradient between the canopy air space (qa) and the mixed layer (qm).

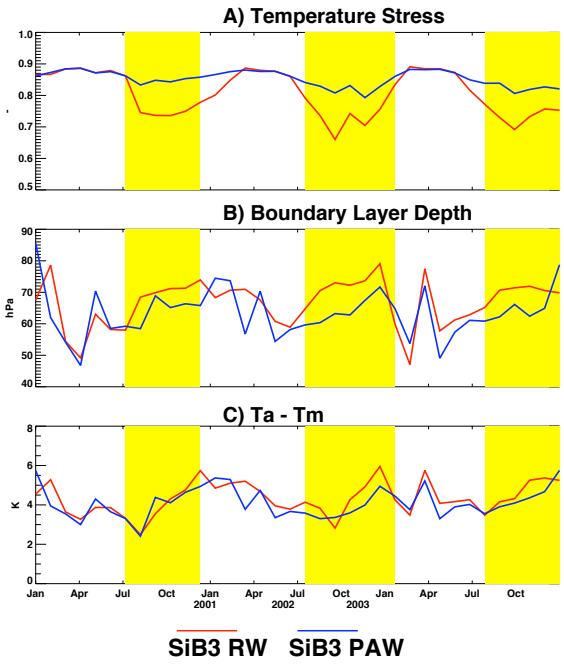

Figure 3.5 Monthly mean values of: A) temperature stress factor, where a value of 1.0 means the plants are completely unstressed. B) Boundary layer depth. C) The temperature gradient between the canopy air space (Ta) and the mixed layer (Tm).

closure, the canopy itself also gets very hot (for example, the month of November 2002 the average canopy temperature was 306 K, with seven days above 320 K), resulting in high sensible heat fluxes and strong canopy heat stress, thereby exacerbating the initial stress imposed on the vegetation.

The seasonal cycle of sensible heat flux is improved using SiB3 PAW, and sensible heat flux is decreased by 1/3 to 1/2 during the dry seasons (Figure 3.3a). Temperatures in the canopy air space, mixed layer, and the canopy itself are all lower in this version compared to SiB3 RW. These factors result in lower temperature stress for the vegetation (Figure 3.5a). The decreased sensible heat flux also reduces the boundary layer depth in SiB3 PAW (Figure 3.5b). These changes have the potential to create less drought-friendly conditions in a full global GCM.

3.3 SEASONAL HYDROLOGIC CYCLE

In the single column model, the balance of moisture in the atmospheric portion of the grid cell is given by Equation 4:

$$\frac{d(PW)}{dt} = LE + \int_{p\_pbl}^{p\_top} \mathbf{V}\nabla q \frac{dp}{g} - P \qquad (4)$$

Where PW = column precipitable water, LE = latent heat flux from the canopy air space to the free atmosphere, and P is precipitation. The vertical integral (from the top of the model to the top of the PBL) of $\mathbf{V}\cdot\nabla$q represents advection into the column.

These quantities are plotted in Figure 3.6. Column water vapor tendency and rainfall are similar between the two models. Also, there is moisture convergence in the rainy season and moisture divergence in the dry season in both models. This is consistent with the observed seasonal migration of the Intertropical Convergence Zone (ITCZ). During the austral fall and winter (ie March through August), the ITCZ results in moisture convergence and convective activity in the equatorial Amazon (Fu et al. 2001). In the austral spring (September through November), the ITCZ migrates to about 10°N, resulting in subsidence and dryness in the northern Amazon (Fu et al. 2001).

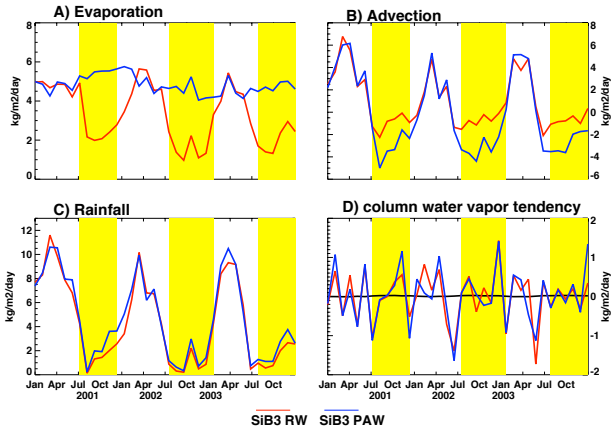

Figure 3.6 A-D) Monthly mean components of the hydrologic cycle. The black line in D represents the residual of subtracting the right hand side of Equation 4 from the left hand side.

The main difference in the water budget is in dry season evaporation and advection. In SiB3 RW, evaporation has a strong seasonal cycle, as discussed above. Dry season moisture divergence is relatively weak and the column water vapor is 1-2 kg/m^2 less in the SiB3 RW atmosphere compared to SiB3 PAW (not shown). Therefore, limited dry season evapotranspiration in SiB3 RW leads to less precipitable water and weaker moisture divergence.

Overall, the hydrologic cycle is stronger in SiB3 PAW. In SiB3 PAW, evaporation is fairly constant throughout the year because of the plants' ability to access deep soil moisture throughout the entire rooting profile. Moisture divergence is about twice as strong in the dry season in this version of the model. During some dry season months (eg: Aug. 2001) the evaporation and advection offset each other, resulting in particularly low rainrates. It is apparent from these plots that SiB3 PAW captures the sustained functioning of the rainforest during the dry season. If anything, the moisture cycling of the forest is overestimated in this version of SiB.

Trenberth (1999) derived a recycling ratio to quantify the percentage of precipitation that results from evaporation from a domain. He also defined a precipitation efficiency and a moistening efficiency. These are:

$$\rho = \frac{EL}{PL + 2F} \qquad I = \frac{PL}{F} \qquad M = \frac{EL}{F} \tag{5}$$

where ρ is the recycling ratio, I is the precipitation efficiency (or the fraction of water vapor over a region that participates in the hydrologic cycle), M is the moistening efficiency (or the fraction of moisture added to the domain through evaporation), E is

total evaporation, P is precipitation, L is the length of the domain, and F is the average horizontal moisture flux through the domain.

These values are shown in Figure 3.7, using a length of 275 km, which is approximately 2.5°. Using a combination of the Climate Prediction Center Merged Analysis of Precipitation (CMAP) data set and NCEP reanalysis data and L of 500 km, Trenberth found that in the equatorial Amazon, moisture transport tends to dominate the recycling ratio. Annual average ρ was about 5%. This is comparable to the moisture recycling in the SCM. During the rainy season, both of the models produce similar results. Precipitation efficiency is high and moisture recycling is approximately 2%. The high horizontal moisture transport into the region is consistent with the location of the ITCZ during these months. During the dry season, the moisture flux decreases by about 100 kg/m/s. However, the vegetation in SiB3 PAW sustains evapotranspiration during the dry season, resulting in a slightly increased recycling ratio and moistening efficiency. The ability of the plants to transpire through the dry season allows the atmosphere to remain moist, and prevents the feedback loop of exacerbating drought through stomatal suicide.

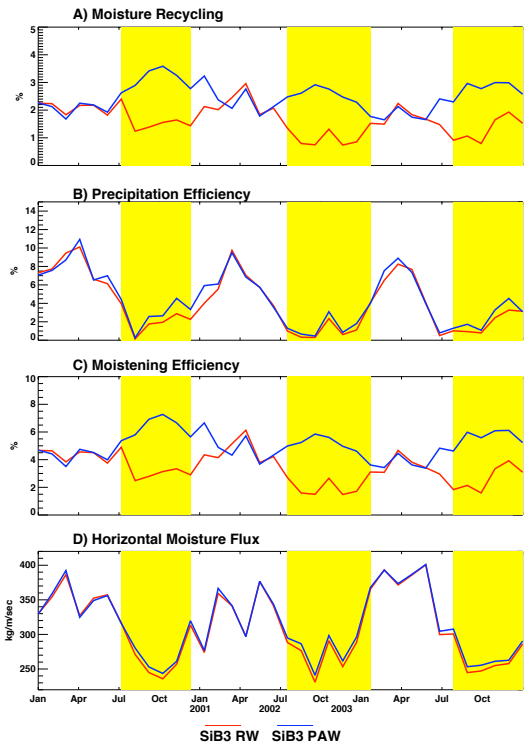

Figure 3.7 Moisture recycling ratio, precipitation efficiency (I), and moistening efficiency (M) calculated u sing a length of 275 km. Using a length scale of 500 km roughly doubles the recycling ratio and efficiencies, however this length is almost twice that of the SCM grid cell. D) F, the horizontal moisture flux across the domain.

3.3 DIURNAL HYDROLOGIC CYCLE

Figure 3.8 shows diurnal averages of precipitation, latent heat, and moisture advection during April and August averaged over 2001-2003. Observed average monthly rainfall was approximately 253 mm and 35 mm during these months, respectively. On an hourly scale, the two versions of the model produce similar results during the month of April. the daytime latent heat flux is overestimated, although the results are still within the range of +/- 1 standard deviation of the observations. According to observations, rainfall at KM83 has roughly two peak periods - one during the night (between 4 and 8 AM) and one in the evening (around 8 PM). Although moisture advection is strongest around midnight (about 9 kg/m^2/day), precipitation doesn't occur until between noon and 8 PM in the model. Moisture convergence has a secondary maximum around noon (4 kg/

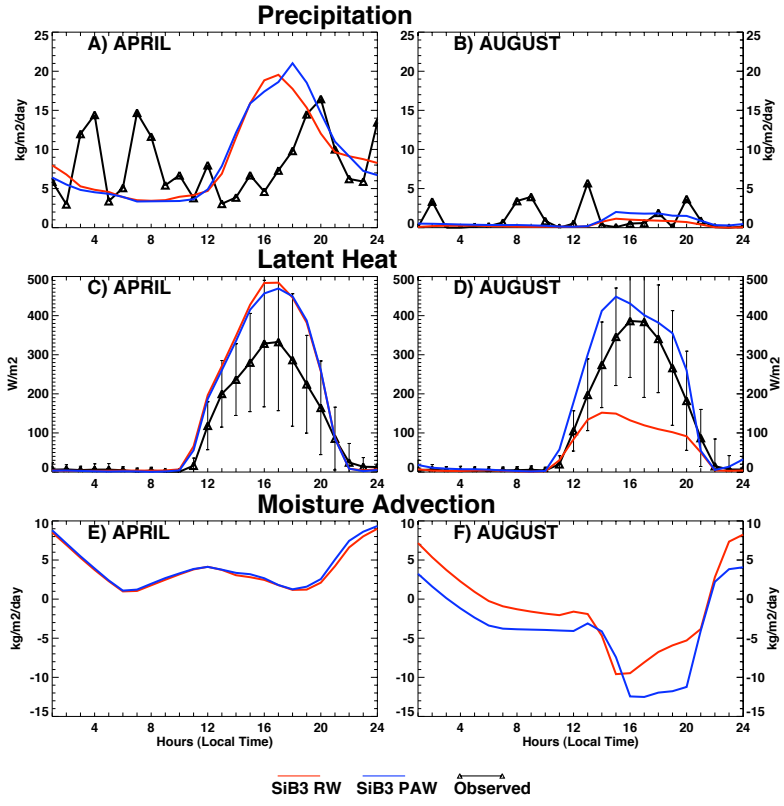

Figure 3.8 Diurnal plots for April and August. Each hour is an average representing the three-year span of the model run (2001, 2002, and 2003). Plots are shown for April, a typically wet month, and August, a typically dry month. The range of +/- one standard deviation for the observations is plotted for latent heat flux. Due to the highly variable nature of precipitation, the hourly standard deviations are larger than the magnitudes of the observations and so are not plotted.

m^2/day), CAPE peaks at 1 PM, and column precipitable water peaks around 4 PM (not shown). Therefore, the atmosphere is gradually storing water throughout the day until the energy necessary for convection is available.

The observed August peak latent heat flux (390 W/m^2) is 118% of the April peak latent heat flux (330 W/m^2). However, the canopy in SiB3 RW does not maintain moisture flux in the dry season - peak latent heat flux in August is only 30% of the peak flux in April. SiB3 PAW shows a large improvement, and during August the peak latent heat flux is about 92% of the April peak.

In August, both models show a divergence of moisture of greater than 5 kg/m^2/ day during the afternoon and evening, roughly during the times of peak latent heat flux. Both models also show convergence during the nighttime. This implies that the column is a source of moisture to the surrounding area during the day and a sink of moisture during the night. In SiB3 PAW, the magnitude of the moisture sink is smaller and the source is larger. In the context of a global GCM, this change would presumably increase the intensity of the hydrologic cycle on a large scale.

3.4 ONSET AND LENGTH OF THE MODELED WET SEASON

Changing root-zone parameters has an effect on the timing and intensity of the wet season. Figure 3.9 shows some statistics for the 2002 and 2003 wet seasons as reproduced by SiB3 PAW and SiB3 RW. Wet season onset is defined in a similar manner

		SiB3 RW	SiB3 PAW	KM83 Obs	NCEP II Reanalysis
2002	**wet season duration**	Jan 25 - June 18	Nov 25-Jun 18	Jan 10 - Jun 28	Feb 4 - Apr 9
	rainrate (mm/day)	7.03	6.37	6.25	7.15
	total precip (mm)	1055	1337	1062	501
2003	**wet season duration**	Jan 10 - May 9	Dec 31- May 9	Jan 25 - Jun 13	Jan 30 - Apr 14
	rainrate (mm/day)	8.14	8.16	6.47	8.27
	total precip (mm)	1018	1102 mm	938	661

Figure 3.9 Timing of wet season onset, and wet season duration, average and total rainfall from two versions of the model and two observational datasets.

as by Li et al. (2004). The onset is the first pentad with greater than 3.33 mm/day of rain, where four of the following six pentads are also above this threshold and four of the previous six pentads are below the threshold.

In SiB3 PAW, the wet season begins earlier and therefore has more rainfall than in SiB3 RW. In 2002, the wet season began two months earlier, and in 2003 it began 11 days earlier. Rainfall intensities from both models are comparable to those observed at the KM83 and from NCEP, but total wet season rainfall from SiB3 RW is closer to observations. The differences in total wet season rainfall results from the length of the season. However, it is interesting that even though the SCM is constrained to the NCEP moisture profile, the changes in root-zone dynamics are able to influence wet season onset.

The factors affecting wet season onset are also different between the models. Figure 3.10 shows the average precipitation, evaporation, and moisture advection during

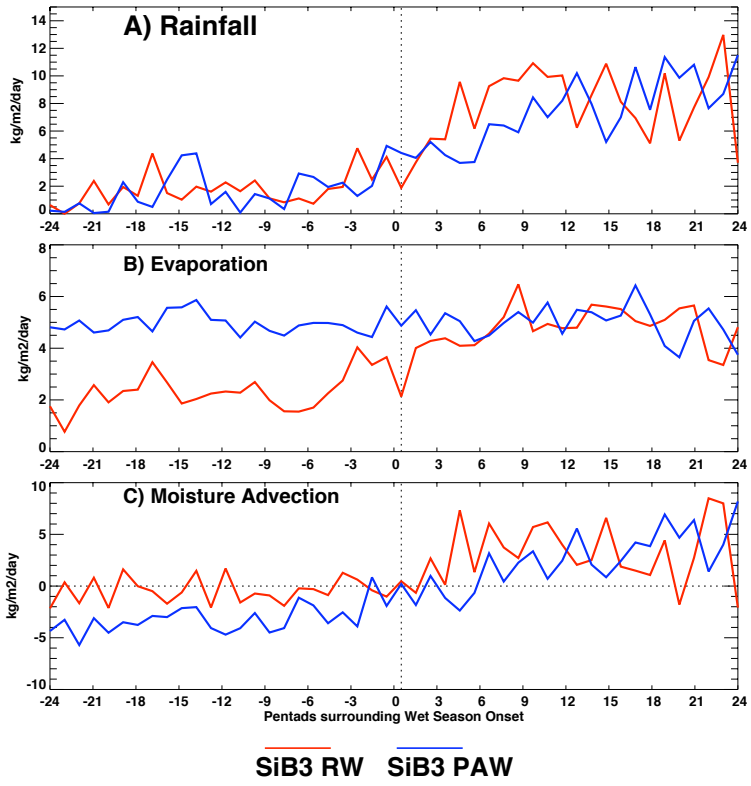

Figure 3.10 Pentad composites of precipitation, evaporation, and moisture advection during the 24 pentads (120 days) preceding and following the wet season onset in 2002 and 2003.

the 24 pentads preceding and following the wet season onsets in 2002 and 2003. The range of dates represented by the 49 pentads are different between the models because they are centered on the onset pentad. In SiB3 RW, the end of the dry season is marked by a combination of weak moisture convergence and divergence. Evaporation increases gradually during the onset period. SiB3 PAW, on the other hand, has strong evaporation even during the dry season. Moisture divergence gradually shifts to weak moisture convergence as the wet season begins. Therefore, surface evaporation has a stronger influence on wet season onset in SiB3 PAW.

4. DISCUSSION AND CONCLUSION

4.1 Implications of decreased soil moisture stress

Figure 4.1 illustrates what the differences between SiB3 PAW and SiB3 RW mean in terms of total monthly rates of precipitation, moisture advection, and evaporation. SiB3 PAW produces more rainfall and stronger evaporation in almost every month. The difference in evaporation is particularly large during the dry season months of July

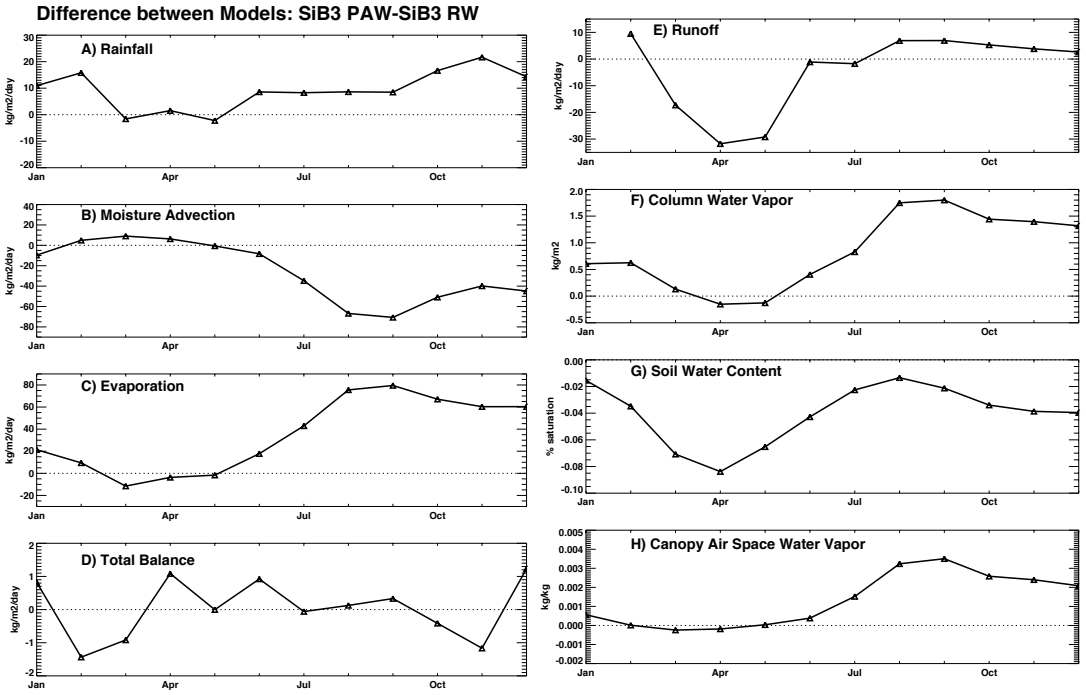

Figure 4.1 Difference in moisture terms between SiB3 PAW and SiB3 RW. A positive difference means that the value is greater for SiB3 PAW. The daily total of each flux and the mean of each storage term was calculated using the three-year average diurnal composites for each month. Each monthly value can be thought of as the area between the SiB3 PAW and SiB3 RW curves on the diurnal plots in Figure 3.8. In D), the total balance refers to the atmospheric budget: Evaporation + Advection - Precipitation. Runoff is not shown for January, when strong runoff in the beginning of the simulation produces unrealistically high runoff.

through December, when it is greater than 40 kg/m^2/day. This flux is of similar magnitude to the actual column water vapor during these months. However, most of the moisture is advected out of the column and does not result in rainfall.

The differences in moisture sources and sinks result in significant variations in total column water vapor. The change in column water vapor is given by the right-hand side of Equation 4, which can be summed up as:

$$\text{Evaporation} + \text{Advection} - \text{Precipitaion}. \quad (6)$$

This sum is shown in Figure 4.1d. During the months of January, April, June, August, September, and December, the sources of moisture to the atmosphere in SiB3 PAW are greater than in SiB3 RW by up to 1.23 kg/m^2/day. During the other months, the SiB3 RW atmosphere has stronger moisture sources by up to 1.43 kg/m^2/day. Over the course of a year, the moisture flux into the SiB3 PAW atmosphere is 19.4 kg/m^2 stronger than to the SiB3 RW atmosphere.

As a result, moisture content in the modeled free atmosphere and canopy air space (Figure 4.1f and h) is greater in SiB3 PAW, particularly during the dry season. The SiB3 RW soil is more saturated and has stronger runoff on a yearly average (Figure 4.1e and g). Runoff is especially strong in wet season months, when it is more than 30 kg/m^2 stronger than in SiB3 PAW. This implies that the shallow soil in SiB3 RW is unable to store much of the rainfall it receives during the rainy season. On the other hand, SiB3 PAW is able to access soil moisture for evapotranspiration, resulting in a smaller percentage of soil moisture lost to runoff.

4.2 Conclusion

This study highlights the importance of root-zone functions in the moisture recycling of the Amazon rainforest. The focus is on how to best represent the soil moisture stress imposed on an ecosystem and the effects of two different representations. Previous versions of SiB and other ecosystem models parameterize root-zone moisture stress based on shallow soils where roots can only access water in their respective layers. However, this study and others (Baker et al. 2008; Liu 2004) show that such parameterizations do not accurately capture the seasonal cycles of heat, moisture, and carbon dioxide fluxes at sites throughout the Amazon. Allowing vegetation to access water throughout the rooting profile has important and interesting effects on land/ atmosphere models. The seasonal and diurnal cycles of fluxes of sensible and latent heat in a version of SiB3 with improved root-zone parameterizations match observations relatively well.

The improved fluxes have the potential to affect the large-scale circulation and hydrologic cycle if implemented into a fully coupled land-atmosphere GCM. For example, stronger evapotranspiration throughout the Amazon basin would result in more precipitable water and possibly more rainfall. The results in Section 3.4 suggest that allowing plants to access deep soil moisture will lengthen and intensify the wet season in the Amazon. Lower sensible heat flux would result in lower surface pressures and a more conducive environment to moisture convergence and convection. In turn, these effects would cause further changes to the large-scale circulation patterns and export of heat and moisture from tropical South America.

Clearly, the changes in SiB3's root-zone calculations has a large impact on the overall moisture of the atmosphere in the single column model. During the dry season, the increased latent heat and decreased sensible heat create a cooler, more moist boundary layer. In turn, the seasonal and diurnal cycles of the column hydrologic cycle are affected, as well as the timing and intensity of the wet season. These effects all occurred within the context of an SCM, where the modeled atmosphere was forced to "relax" toward the upstream observations. The next step is to implement SiB3 PAW into a GCM. This will have interesting and important impacts the large-scale dynamics through large-scale interactions between the land surface and the atmosphere.

III. PART TWO:

How do deep roots in the Amazon affect the regional climate?

1. INTRODUCTION

Land-atmosphere interactions have significant effects on both weather and climate. Land surface sensible and latent heat fluxes feed back to the large-scale circulation through boundary layer convection and radiative forcing. In turn, the atmospheric conditions have a strong influence on the vegetation's health. Plants have developed sophisticated methods to survive drought, but there is a limit to what they can withstand. Therefore, as the global climate changes, it is important to understand these interactions.

A region of particular interest is the Amazon rainforest. The effects of both global warming and land use change are predicted to cause a drier climate in this region (Oliveira et al. 2005). Current coupled carbon-climate models and observations portray varying degrees of the forest's ability to adapt to climate change. In several models, the rainforest is limited by water availability and severe Amazonian drought stress is predicted (ie: Cox et al. 2004; Friedlingstein et al. 2001; Lui et al. 2004). On the other hand, observations suggest that the forest is light-limited and somewhat resistant to short-term drought (ie: Huete et al. 2006; Saleska et al. 2003; Nepstad et al. 2002; Brando et al. 2008).

It is important to determine how resistant the rainforest is to drought. The models are predicting stress to an extent that we have not yet seen in the present-day Amazon. Is

this stress realistic? What is causing it? Furthermore, how does the vegetation cope with short-term drought? In this study, we propose that uncertain soil and root parameterizations in the models lead to extreme drought stress. By allowing the vegetation in a coupled model to access deep soil moisture in a more realistic manner, we will study the effects of root zone stress on the climate. In this way, we can determine if the catastrophic results predicted by the models are realistic.

OVERVIEW OF MODEL RESULTS

First, we examine the models that predict Amazonian drought stress. In particular, two studies found decreases in forest productivity due to increased atmospheric CO_2 in the atmosphere. Cox et al. (2000, 2004) coupled an ocean-atmosphere GCM (HadCM3) to a dynamic vegetation model (TRIFFID). In the 21st century, a warming pattern emerged over the Pacific. The pattern, which included greater warming over the Eastern Pacific, resembled conditions during El Nino, when rainfall is typically reduced in northern Brazil (Cox et al. 2004).

In TRIFFID, the vegetation can change in response to climate change. The coupled model of Cox et al. predicted a transition from forest to savannah throughout the entire Amazon due to soil moisture limitations on photosynthesis and increasing maintenance respiration costs (Cox et al. 2004). Similar results, but of smaller magnitude, were found by Friedlingstein et al. (2001), using the ISPL ocean-atmosphere GCM coupled to a terrestrial carbon model (SLAVE). Unlike in TRIFFID, the vegetation in SLAVE is prescribed, so no dieback occurred. However, net ecosystem production (NEP)

was reduced in South America due to an increase in soil aridity due to increased evaporative demand.

This study uses the Simple Biosphere model (SiB3) coupled to CSU's GCM (BUGS5) to investigate the effects of soil moisture stress under current climate conditions. Previously coupled runs of SiB/BUGS have had problems simulating the Amazon hydrologic cycle. The first coupling of SiB with a GCM occurred in 1986, when its first version (SiB1) was incorporated into the UCLA/GLA GCM. As described by Randall et al. (1996), the soil dried out over the first two simulated years and modeled continental evaporation and precipitation were much less than observations. The cause was deemed to be excessive stomatal closure due to environmental stresses. Randall et al. called this phenomenon "stomatal suicide."

The next version of SiB (SiB2) attempted to better simulate the simultaneous transfer of CO_2 into and water vapor out of the vegetation through a canopy photosynthesis-conductance model (Sellers et al. 1996; Denning et al. 1996; Randall et al. 1996). Although stomatal suicide was absent, the SiB2-GCM boundary layer was too warm and dry during July in the Amazon, resulting in overestimated sensible heat and underestimated latent heat. The simulated soil moisture in the top two layers also showed a weak drying trend over the ten-year simulation (Randall et al. 1996). In particular, SiB2 simulated extreme drought stress during the dry season at two sites in the Amazon, which is inconsistent with observed data (Liu 2004). Liu's experiments showed signs of stomatal suicide through a drying of the Amazon region over a three-year simulation until ultimately the Amazon hydrologic cycle was shut down.

The biophysics behind stomatal suicide are realistic, but it is unlikely that it would occur as intensely as in the coupled model. Vegetation responds to a warm and dry boundary layer by increasing its stomatal resistance, which limits the rate of evapotranspiration and allows the plants to conserve water. The decreased evapotranspiration warms and dries the PBL, leading to a further increase in stomatal resistance and a further decrease in evapotranspiration. Also, increased surface sensible heat causes the PBL to deepen, which could create persistent high surface pressure and/or a pressure ridge. These effects also serve to exacerbate drought conditions. This positive feedback loop could eventually cut off all evapotranspiration and create a boundary layer that is too hot and dry to sustain the vegetation. In the extreme case, rainfall is cut off because advected moist air masses are diluted in the warm, dry, and deep boundary layer. This prevents the boundary layer from reaching a critical mixing ratio to trigger precipitation in the model. In reality, vegetation can survive episodes of warm, dry weather because it has an upper limit on stomatal resistance and a lower limit on evapotranspiration (Randall et al., 1996).

OVERVIEW OF OBSERVATIONS

These three modeling studies simulated drought stress in the Amazon due to inadequate soil moisture. In contrast, several observational studies have found that the rainforest is more limited by light than by water and therefore has the ability to thrive through seasonal dry periods. For example, the MODIS Enhanced Vegetation Index (EVI), measured from 2000 to 2005 across the Amazon Basin, increased by 25% during the dry season in forests (Huete et al. 2006). Calculations of EVI use near-infrared

radiation and can be used to estimate area-averaged canopy photosynthetic capacity and gross primary production (GPP) (Sellers et al. 1992; Rahman et al. 2005). The concept of dry season greenness is supported by measurements of gross primary production (GPP) by eddy flux towers in the Tapajos National Forest (Huete et al. 2006; Saleska et al. 2003).

During the dry season, assimilation of carbon by the plants is encouraged by the abundance of photosynthetically active radiation (PAR). However, plants' stomatal opening is regulated both by the need to assimilate carbon dioxide and to limit water loss. Therefore, roots that can access soil moisture during dry periods are essential to a plant's survival of dry periods. In the Amazon, trees can have tap roots that extend very deep into the soil. Roots have been observed up to 11 m deep (Nepstad et al. 1994; Jipp et al. 1998; Nepstad et al. 2002). Through hydraulic redistribution, water moves through the roots along the water potential gradient, to supply moisture to the canopy when the air is dry. It can also work in the reverse to replenish deep soil water during a rainfall following a rainless period, for example (Oliveira et al. 2005). Hydraulic redistribution not only increases a plant's drought tolerance, it also enables the plant to maintain transpiration and carbon sequestration during seasonal droughts (Oliveira et al. 2005). Incorporation of hydraulic redistribution into the NCAR Community Land Model led to increased dry season evapotranspiration and decreased temperatures in the Amazon, which affected the global climate (Lee et al. 2005).

Although hydraulic redistribution is clearly an important process on short time scales, it cannot protect the vegetation from drought stress indefinitely. This was shown

through a rainfall-exclusion study in the Tapajos National Forest in Brazil. From 2000 through 2004, wet season rainfall was excluded from a 1 ha plot, resulting in a reduction in rainfall reaching the soil of 35-41% (Figure 1.1). Initially, the forest was resistant to the imposed drought. After the first year, there were relatively low reductions in wood production (13%), leaf area index (LAI), and above-ground net primary productivity (ANPP) (12%) (Brando et al. 2008). There was no detectable increase in leaf drought stress (Nepstad et al. 2004).

However, over the following four years, results showed that the rainforest is affected by multi-year droughts. Total wood production and ANPP decreased by up to 63% and 41%, respectively. Other changes were an inhibited formation of new leaves, a decrease in surface (0-2 m) and deep soil (2-11 m) water content, reduced photosynthetic capacity, stem radial growth, fine litterfall, and fruiting (Nepstad et al. 2004). Overall, 9% of the trees on the exclusion plot died over the five-year experiment. In 2005, the first year of recovery, litterfall fully recovered and wood production rebounded to only 13% less than the control plot (Brando et

Figure 1.1 Panels prevent rainfall from reaching the forest floor in the rainfall exclusion experiment. View from above (top) and below (bottom) the panels. Photo courtesy Woods Hole Research Center.

al. 2008).

From this discussion, we can draw a few conclusions. First, both the models and the observations highlight the sensitivity of the forest to extended drought. Second, coupled carbon/climate models are increasing our understanding of the effect of the Amazon on large-scale atmospheric features. In the models, soil moisture stress leads to decreases in forest productivity and interactions between the land and atmosphere that tend to intensify and extend drought. However, observations show an amazing resilience in the forest to withstand periods of drought and suggest that the forest is more light-limited than water-limited. This leads to the final conclusion that further model development is needed for coupled carbon/climate models.

Recent model developments with SiB have improved our ability to simulate fluxes of heat, moisture, and carbon at several sites in the Amazon (Baker et al. 2008; Harper et al. 2008). We have shown that incorporating the changes in SiB into a single column model of the CSU GCM (BUGS5) create more realistic results at an eddy flux tower in the Amazon. Therefore, the next logical step is to run the model in the global GCM, which enables us to analyze large-scale land-atmosphere interactions.

In this paper, we will show results from coupling the most recent versions of SiB into BUGS5. In Section 2, some background information on Amazon climatology, moisture recycling, and upper tropospheric conditions is given. In Section 3, the models, their coupling, and the treatment of soil moisture stress in SiB are discussed. In Section 4, results are given for the coupled GCM. Important implications of this study and future work are discussed in Section 5.

2. BACKGROUND

2.1 OBSERVED CLIMATOLOGY OF THE AMAZON BASIN

Observed rainfall in the Amazon primarily comes from networks of rain gauges and satellites. The Global Precipitation Climatology Project (GPCP) is a precipitation data set from 1979 to the present that uses a combination of rain gauge and satellite data (Huffman et al. 1997). Reanalysis, such as NCEP and ECMWF, uses observed temperature, humidity, and wind profiles to drive models that produce spatially and temporally homogenous rain rates. For this study, we examine the monthly mean precipitation on a 2.5°x2.5° grid from both data sets. Water vapor and temperature from the lower atmosphere are also used from NCEP2 to compare to model results. Annual average precipitation rates in the Amazon River basin from GPCP (1988-1995) and NCEP Reanalysis (1976-1996) are 5.19 mm/day and 6.36 mm/day, respectively (Costa and Foley, 1998). A handful of other observational datasets have rain rates that fall between these two values (Costa and Foley 1998). On a spatial basis, the rain rate has been found to vary from less than 5.5 mm/day in the southern, eastern, and extreme northern basin to greater than 8.2 mm/day in the northwestern basin with a secondary maximum near the mouth of the Amazon River (based on rain gauges, Liebmann and Marengo, 2001).

The rainy season occurs at different times in the northern and southern Amazon. During the austral fall and winter, the Intertropical Convergence Zone (ITCZ) results in convective activity in the equatorial/northern Amazon (Fu et al. 2001). In the austral spring, the ITCZ migrates to about 10°N, resulting in subsidence and dryness in the northern Amazon (Fu et al. 2001). During the austral spring and summer, low level northerly flow, which imports atmospheric moisture from the Atlantic, and upper-level anticyclonic flow (the Bolivian high) enhances low level convergence and hence fuels the southern Amazon rainy season (Wang and Fu 2002).

In order to study the conditions during wet and dry seasons, we derive a method for determining wet and dry months in these two datasets (a similar method is used in the results section with the model output). For each dataset, the mean precipitation rate for the region depicted in Figure 2.1 is found. The wet (dry) months are defined as months with greater than (less than) the mean plus (minus) half the standard deviation. (The standard deviation is based on monthly deviations from the area-averaged mean). It is common to define the dry season as months with less than 100 mm of rainfall (e.g. Huete et al. 2006). However, with this definition one of our models would not have a dry season in the northern Amazon (see Figure 4.9). This would not allow us to examine results during the dry season. Therefore, we chose a definition of wet and dry months that selects the relatively wettest and driest months in each dataset and in the results.

The wet months tend to fall from November to March, and the dry months tend to fall between June and September, although this varies slightly from year to year. As it turns out, the dry months occur when rainfall is higher in the northern Amazon and the

wet months occur during the southern Amazon's rainy season. The composites of observed wet and dry monthly rainfall are shown in Figure 2.1. According to GPCP, during the Amazon dry season, there is less than 2 mm/day of rainfall throughout large areas of the southern Amazon region and in southeastern Brazil. The signature of the ITCZ can be seen north of the equator, where rainfall reaches almost 10 mm/day. The pattern is similar in the NCEP2 rainfall, except for a greater intensity of rainfall in the northern Amazon.

During the Amazon rainy season, rain rates are above 7 mm/day throughout much of the central basin. In the GPCP data, there are two regions with maximum rainfall – one

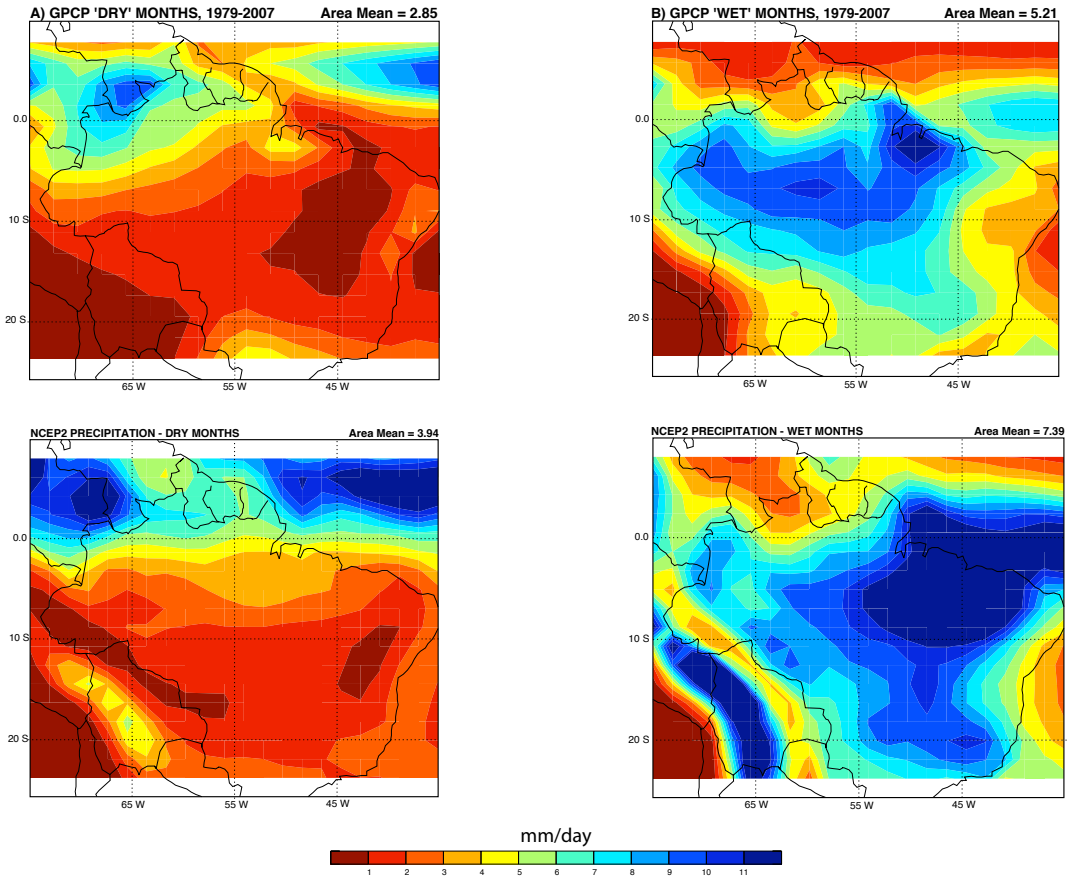

Figure 2.1 Monthly composites of rainfall during wet and dry months from the Global Precipitation Climatology Project data set and from NCEP 2 Reanalysis, from 1979 to 2007.

in the central basin and one near the mouth of the Amazon River. In NCEP2, rainy season rainfall is much stronger, with large areas receiving more than 11 mm/day. The peak rainfall occurs in northeastern Brazil and extends through the southern Amazon and southeastern Brazil.

At some points in this study, we differentiate between the southern and northern (or equatorial) Amazon regions. Following Li and Fu (2004), we define the southern Amazon region as 5°S to 15°S and 45° to 75° W. The northern Amazon region is defined as 10°N to 5°S and 45° to 75° W (see Figure 3.3). The wet and dry seasons are of

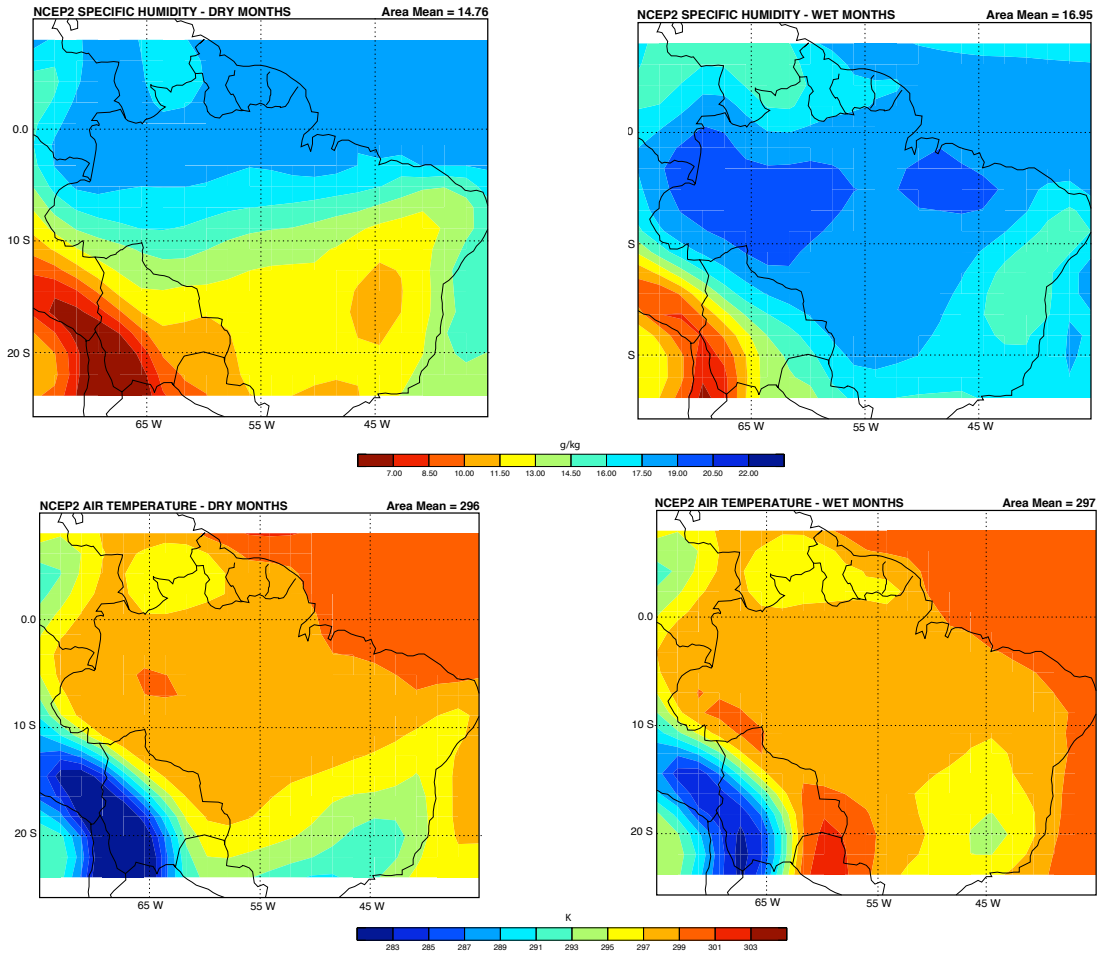

Figure 2.2 Specific humidity (g/kg) and temperature (K) from NCEP 2 Reanalysis during wet and dry months from 1979 - 2007. For specific humidity, blues indicate more moisture, while for temperature the blues indicate cooler temperatures.

opposite phase in the two domains, and the dry season in the southern Amazon is much drier and more widespread than in the northern Amazon.

NCEP2 surface specific humidity and air temperature are shown in Figure 2.2. During the dry season, there is a swath of relatively cool, dry air extending from the southwest to the northeast. Specific humidity is highest in the northern Amazon, where strong precipitation is occurring. The majority of the Amazon basin also has a higher specific humidity during the rainy season. Temperatures in the Amazon basin are typically between 297 to 300 K during both seasons.

2.2 AMAZON MOISTURE RECYCLING

Amazon rainfall depends on moisture advected into the region from the Caribbean Atlantic and on local evaporation. Spatially, local evaporation increases in importance in the southern and western portions of the basin, or regions farther from the influence of moisture transport (Eltahir and Bras, 1994). In this study, we use the equations of Trenberth (1999) to calculate recycling ratio (ρ), precipitation efficiency (*I,* the fraction of water vapor over a region that participates in the hydrologic cycle), and moistening efficiency, (*M,* the fraction of moisture added to the domain through evaporation).

$$\rho = \frac{EL}{PL + 2F} \qquad I = \frac{PL}{F} \qquad M = \frac{EL}{F} \tag{1}$$

where *E* is total evaporation, *P* is precipitation, *L* is the length of the domain, and *F* is the average horizontal moisture flux through the domain and

$$F = \int_{p\_sfc}^{p\_top} qV \frac{dp}{g} \qquad (2)$$

where q is the specific humidity and V is the magnitude of the horizontal wind field.

In the equatorial Amazon, moisture transport tends to dominate the supply of atmospheric moisture and the recycling ratio is less than 20%, while in the southwestern corner of the basin it reaches 50% (Eltahir and Bras, 1994). Annual average moisture recycling has been calculated to be between 25 and 35% (Trenberth, 1999; Eltahir and Bras, 1994; Costa and Foley, 1999), depending on the observational data set used, time period considered, and definition of the recycling ratio.

Therefore, the area-averaged annual evaporation in the Amazon contributes to anywhere from one-quarter to one-third of the region's precipitation. This value changes in space and time, for example it is larger in the southern Amazon during that region's rainy season. This indicates that the northern Amazon rainy season is mostly influenced by moisture transport, and there is a larger contribution from evaporation in the southern Amazon. We expect to see a shift in the importance of local evaporation between the two models.

2.3 OBSERVED UPPER TROPOSPHERIC CONDITIONS

In the upper troposphere, the wet season in the Amazon is characterized by the presence of a region of raised geopotential heights (the Bolivian high) and associated anticyclonic flow, and a trough located downstream of the high (the Nordeste low). The Bolivian high is typically centered between 10° and 20°S and near 60° to 65°W (Horel et

al. 1989; Lenters and Cook 1997; Li and Fu 2004) (See Figure 1 in Horel et al. 1989). During the wet season, heavy convection, as indicated by observed OLR of less than 200 $W/m^{2,}$ occupies most of the Amazon basin south of the equator. Downstream (east) of the high, a trough coincides with the maximum area of convection (Horel et al. 1989). During July, the region of low OLR shifts to a zonal band centered on 10°N and extending from roughly 60° to 120°W. The southern Amazon is characterized by zonal westerlies at 200 mb and the Bolivian high and trough are no longer present (Horel et al. 1989).

The presence of the Bolivian high is mostly attributable to mid-tropospheric heating due to condensation, although topography and thermal transients also play a role (Lenters and Cook, 1997). Linear modeling studies, such as those done by Silva Dias et al. (1983), suggest that the high is a manifestation of southwestward propogating Rossby waves in the upper troposphere, which are a response to condensation heating above the Amazon basin. Lenters and Cook (1997) found that the positioning of the Bolivian high is most strongly influenced by precipitation in the Amazon, while its strength is largely due to rainfall in the central Andes. Sensible heat flux from the elevated terrain of the Andes has a minimal direct effect on the Bolivian high.

Because the Bolivian high develops following wet season onset, it seems to be a result of, and not the cause of, Amazon rainfall (Horel et al. 1989; Lenters and Cook 1997; Li and Fu 2004). According to ECMWF reanalysis, geopotential heights at 200 mb increase leading up to wet season onset. About one month before the onset, upper tropospheric anticyclonic circulation begins to form southwest of the Amazon basin. As

peak rainfall moves from the equatorial Amazon and northern South America, the anticyclonic circulation also moves southward and intensifies. It grows stronger following wet season onset. This circulation feature is related to the Bolivian high, and combined these two features lead to rotational kinetic energy and divergence in the upper troposphere. These features are similar to those of the south Asian monsoon (Li and Fu 2004). They are important for the onset and sustenance of the Amazon rainy season.

This upper tropospheric set up of the rainy season can be disrupted by shifts in the ITCZ during the austral spring and by warmer than usual SST's in the Pacific cold tongue region (El Nino). The former affects the Hadley Cell while the latter affects the Walker circulations. Both cases result in subsidence over the Amazon basin, resulting in low-level anticyclonic flow and reduced precipitation (Fu et al. 2001). This would show up in the upper troposphere as regional divergence and lowered geopotential heights. Such a situation would decrease precipitation and potentially trigger interactions between the land and atmosphere (ie: stomatal suicide) which could exacerbate the drought. Therefore, it is important for the model to capture the upper level circulation features.

Lenters and Cook (1997) also found that the circulation around the Nordeste low is mostly due to condensation heating above the Amazon and the South Atlantic Convergence Zone (SACZ). Interestingly, they found that the eastern part of the low (where the flow is northerly) is influenced by precipitation downwind in Africa. Because these upper tropospheric circulation patterns are important aspects of precipitation over South America, it is important for the model to capture them, and it is of interest to see how they are affected by surface processes.

3. METHODS

3.1 MODEL DESCRIPTIONS

SiB

The Simple Biosphere (SiB) model is based on a land-surface parameterization scheme that computes biophysical exchanges (Sellers et al. 1986) and ecosystem metabolism (Sellers et al. 1996a; Denning et al. 1996). Photosynthetic carbon assimilation is parameterized based on the enzyme kinetics of Farquhar et al. (1980) and is linked to the surface energy budget and atmospheric climate via stomatal conductance (Collatz et al. 1991, 1992; Sellers et al. 1996a; Randall et al. 1996). SiB calculates fluxes of heat, moisture, momentum, and CO_2 from the gradients of each between the canopy air space and the free atmosphere, scaled by a resistance.

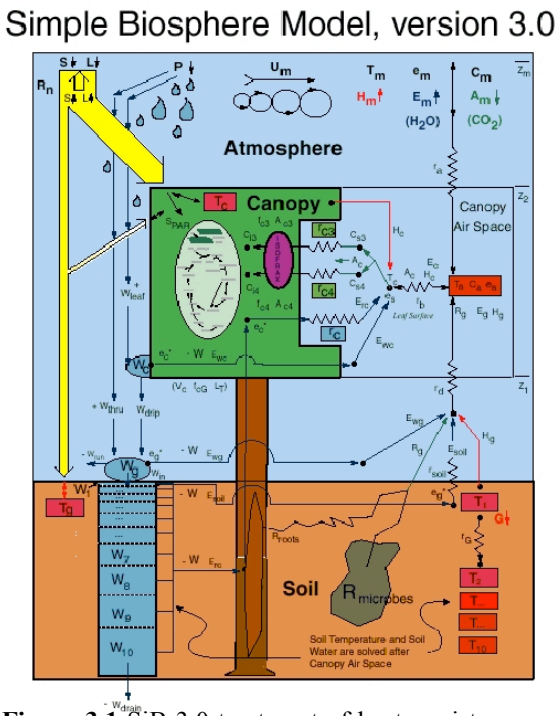

Figure 3.1 SiB 3.0 treatment of heat, moisture, and carbon dioxide fluxes from the ground and the canopy.

In this study, two different set-ups of SiB3 coupled to a GCM are compared: 1) a version of SiB3 with soil moisture stress calculated using root-

weighted stress (SiB3 RW) and 2) SiB3 with deep roots and soil moisture stress calculated using plant available water (SiB3 PAW).

SiB3.0 using a root-weighted stress calculation (SiB3 RW)

SiB3 RW includes a 3.5 meter deep, 10 layer soil with a water extraction root profile extending through all layers (Figure 3.1). This change is adapted from the Community Land Model (Dai et al. 2003) and based on the earlier NCAR Land Surface Model (Bonan 1996). Soil moisture stress is calculated layer-by-layer and is weighted by the fractional amount of roots in each layer. In the canopy air space (CAS), temperature, water vapor, CO_2, heat and water fluxes are predicted from time step to time step.

SiB3 using plant available water to calculate stress (SiB3 PAW)

In this model, which is also fully described in Baker et al. (2008), soil depth is increased from 3.5 meters to 10 meters. Also, plant available water (PAW) replaces root-density weighted water to calculate water stress.

BUGS5

BUGS5 is an atmospheric general circulation model that has evolved from the 1980's UCLA GCM. The model uses an explicit planetary boundary layer (PBL) depth with prognostic turbulent kinetic energy. The PBL is the lowest level in the model, which uses a modified sigma coordinate (Suarez et al. 1983; Randall et al. 1985).

The radiation parameterization in the GCM utilizes a 2-stream method for calculating broadband and heating rages in the shortwave and longwave and accounts for IR scattering (Stephens et al. 2001; Gabriel et al. 2001). The cumulus cloud parameterization includes ice phase microphysics, prognostic convective closure, and

multiple cloud-base levels (Arakawa and Schubert 1974; Randall and Pan 1993; Pan and Randall 1998; Ding and Randall, 1998). The stratiform cloud parameterizations include prognostic cloud droplets, ice crystals, and hydrometeors (Fowler et al. 1996; Fowler and Randall 2002). BUGS5 uses a dynamical core based on a spherical geodesic grid (Ringler et al. 2000; Randall et al. 2002).

3.2 ROOT-WEIGHTED VERSUS PLANT AVAILABLE WATER STRESS

SiB calculates a potential photosynthetic rate that is dependent on factors such as leaf area, CO2 concentration at the leaf surface, and radiation absorbed by the canopy. Potential photosynthesis is then scaled by three stress factors in order to maximize carbon assimilation while minimizing water loss. Stress can originate from less than optimal temperature, humidity, and soil moisture. This study focuses on the latter.

Figure 3.2 shows treatments of root depth and density in SiB3 RW and SiB3 PAW. SiB3 PAW corresponds to the deep soil SiB3 discussed in Baker et al. (2008). Root depth is 3.5 and 10 meters in SiB3 RW and SiB3 PAW, respectively, allowing the latter version of the model to hold more water in the soil. Furthermore, the removal of transpired water is treated differently. In SiB3 RW, transpired water is removed from the soil based on actual root fractions in each layer (Figure 3.2a). While this seems physically realistic, it does not take into account hydraulic redistribution, which is essentially the ability of roots to move water to and from areas of water deficit and surplus (Oliveira et al. 2005). In SiB3 PAW, transpired water is removed from an “apparent” root fraction, which takes into account both actual root fraction (Figure 3.2c) and moisture content (Figure 3.2d) in

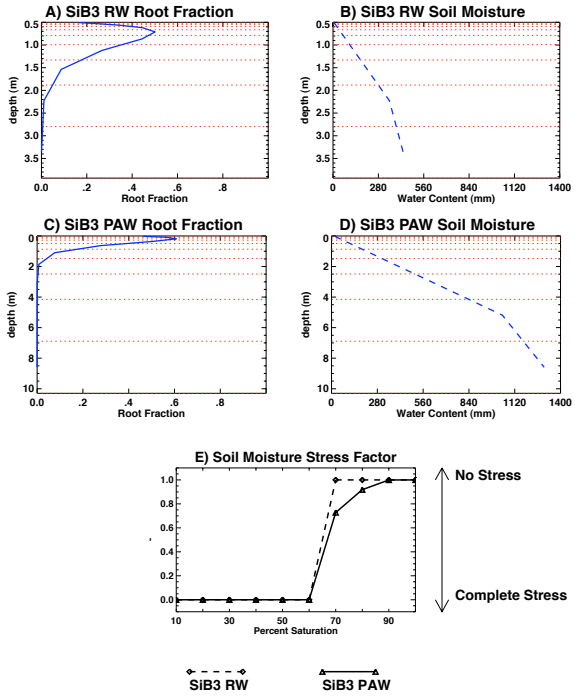

Figure 3.2 Treatments of roots and soil moisture stress within SiB3 RW and SiB3 PAW. The soil depth is increased throughout all of SiB3 PAW, but the rooting density shown here only applies to the broadleaf evergreen biome. Soil moisture is at 90% saturation (b & d).

each layer. As is shown in Figure 3.2 (b & d), the most water resides in the deepest layers. Although root density is low in these layers, it is greater than zero. Therefore, in SiB3 PAW, the vegetation is able to access moisture throughout the rooting profile. This new calculation of soil moisture stress is a function of plant available water within the entire rooting profile, independent of layer-by-layer moisture content or root fraction. The ability of deep roots to access large amounts of water has been observed by Jipp el al. (1998) and Nepstad et al. (1994).

Furthermore, this treatment acts as a parameterization of hydraulic redistribution (HR). HR has been found to be an important inclusion in models for simulating dry season evapotranspiration in the Amazon (Lee et al. 2005; Baker et al. 2008). In a similar study using a single column model of BUGS/SiB, sensible and latent heat fluxes from SiB3 PAW were comparable to a version of SiB3 with HR (Harper et al. 2008). Using

single-point runs of offline SiB3, Baker et al. (2008) found that SiB3 PAW (called SiB3 deep soil in the paper) had a similar photosynthetic response to SiB3 with HR, but different respiration. However, coding of HR in SiB requires an empirical conductivity factor for which global data is not available.

Another key difference between SiB3 RW and SiB3 PAW is the calculation of soil moisture stress (Figure 3.2e). The soil moisture stress factor is calculated so that a value of 1.0 means there is no stress on the vegetation from soil moisture, while a value of 0.0 means the vegetation is completely stressed by lack of soil moisture. In both versions of the model, plants will not transpire when water content is below the wilting point and slight stress is imposed when moisture is below field capacity. Stress slowly increases in SiB3 RW until just above the wilting point, at which point it increases rapidly. Although this response is realistic on a plant-to-plant basis, a smoother response is more realistic on the scale of a grid cell. Therefore, in SiB3 PAW, stress increases more gradually below field capacity.

3.3 COUPLED MODEL SET-UP

The geodesic grid solves vorticity and divergence equations rather than the momentum equation. Analytic horizontal operators are numerically solved with second-order accuracy. This experiment used a resolution of 2562 polygons, equivalent to 4.5° x 4.5°. The geodesic grid combines advantadges of both spectral models and traditional finite-difference models. For example, polygons are nearly uniform over the entire globe - the ratio of the smallest to largest grid cell size is 0.948 (Ringler et al. 2000; Randall et

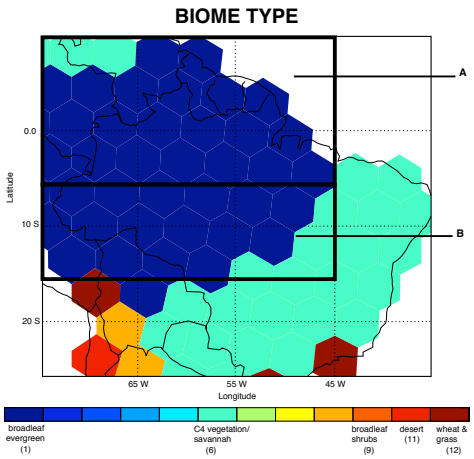

Figure 3.3 Dominant vegetation types in the Amazon region - defined as 10°N to 25°S and 75°W to 35°W. Domain A is the northern Amazon (10°N to 5°S and 75°W to 45°W) and domain B is the southern Amazon (5°S to 15°S and 75°W to 45°W).

al. 2002). The sea surface temperatures are average monthly values from 1956 to 2000 based on AMIP II observations (Taylor et al. 2001; Fiorino 2000).

SiB3.0 specifies vegetation and soil parameters as monthly values based on vegetation type and satellite-derived vegetation data. The parameters were specified using a combination of land cover type (Hansen et al., 2000), monthly maximum normalized difference vegetation index (NDVI) derived from advanced very high-resolution radiometer (AVHRR) red and near-infrared reflectance (GiMMSg - Brown, 2004; Tucker et al. 2005; Pinzon et al. 2006), and soil texture (Tempel et al. 1996). Time-invariant vegetation biophysical parameters such as canopy height, leaf angle distribution, leaf transmittance, and parameters related to photosynthesis are based on values recorded in the literature and assigned via look-up tables (Sellers et al., 2006b). In all biome types except for broadleaf-evergreen, time-varying vegetation biophysical parameters such as fraction of photosynthetically active radiation (FPAR), fraction of vegetation cover, greenness fraction, and leaf area index (LAI) are calculated from one year of NDVI monthly maximum value composites for the site (Sellers et al. 1996b; Los et al. 1994). The NDVI has been adjusted in order to account for cloud contamination, atmospheric effects, off-nadir viewing, and erroneous data (Sellers et al. 1996; Holben

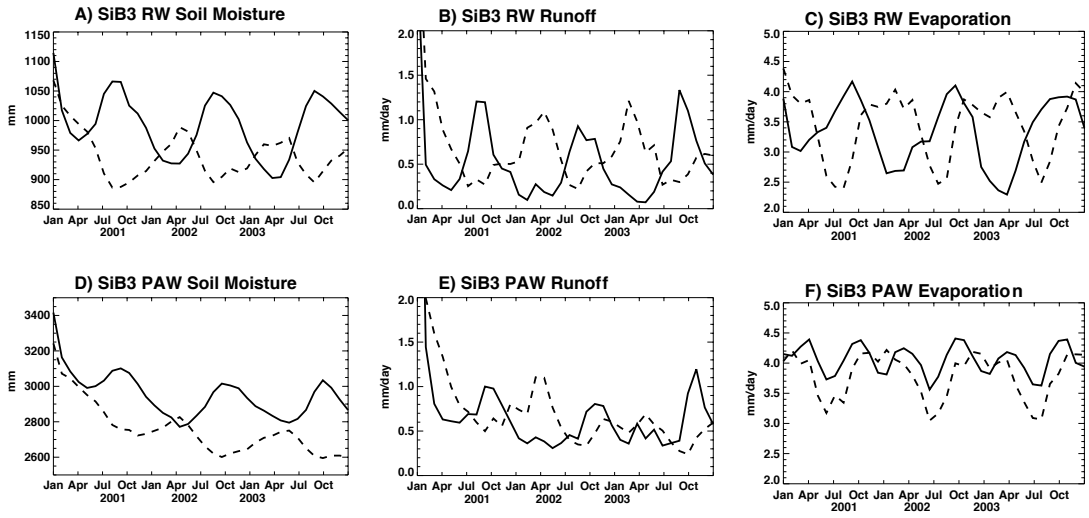

Figure 3.4 Monthly mean average grid cell soil moisture (a,d), total runoff (b,e) and total evaporation (c,f) for the Amazon region from 2001 to 2003. Both models are initialized at 90% saturation but SiB3 PAW has a deeper soil and thus more soil moisture.

1986; Los et al. 1994). For tropical forest points, the maximum value from a 20-year record of NDVI monthly maximums is used in order to reduce the effect of atmospheric scattering, absorption and particularly clouds. Soil hydraulic and thermal parameters are calculated from the percent of sand and clay in the soil using equations from Clapp and Hornberger (1978).

SiB3 ran for 20 years to initialize surface variables of CO_2, temperature, and soil moisture. Where the dominant vegetation type is broadleaf evergreen (Figure 3.3), initial soil moisture content was set to 90% saturated. The coupled model was then run for 3 years, from 2001 to 2003.

Because soil moisture was initialized at 90% in some places, we want to ensure that this did not result in spurious evaporation rates. Effects of initial soil water content is examined in Figure 3.4. Soil moisture for the northern and southern Amazon rainforest is shown in this figure. Throughout most of 2001, the soil moisture is decreasing from its

initial value of 90% saturation. This water could be either evaporating or exiting the grid cells through runoff. Figure 3.4 (b & c) show that most of the water loss in the beginning of 2001 goes into runoff and not into the atmosphere. An exception is elevated evaporation in January 2001 in the southern Amazon in SiB3 RW. In 2002 and 2003, soil moisture returns to similar levels during each region's wet season. Here the exception is SiB3 PAW in the southern Amazon. During the wet season of 2002, soil moisture reaches a peak in April in this region. However, a similar pattern in the runoff indicates that excess soil moisture is not going into the atmosphere.

4. RESULTS

We now discuss how the different treatments of soil moisture stress and soil depth in the model affect vegetative stress, surface fluxes, boundary layer meteorology, the hydrologic cycle, moisture recycling, and upper tropospheric circulation. As with GPCP and NCEP2, we define wet (dry) months as months with greater than (less than) the mean precipitation for both sets of results plus (minus) half the standard deviation. Similar to the observations, wet months tend to fall from November through March, and dry months tend to fall from May through August.

4.1 SOIL MOISTURE STRESS AND SURFACE FLUXES

In SiB3 PAW, soil moisture stress is greatly decreased throughout tropical South America (Figure 4.1). In SiB3 RW, the soil moisture stress roughly follows the pattern of the precipitation, indicating that once the rain stops the plants do not have enough soil moisture to continue transpiration and photosynthesis. However, in SiB3 PAW, there is very little difference in the maps of soil moisture stress factor between the wet and dry months. This indicates that the roots are able to access soil water even when the rain stops. Another important difference between the two models is that in SiB3 PAW, almost the entire basin is unstressed. This allows the vegetation throughout the region to function during both the wet and dry seasons.

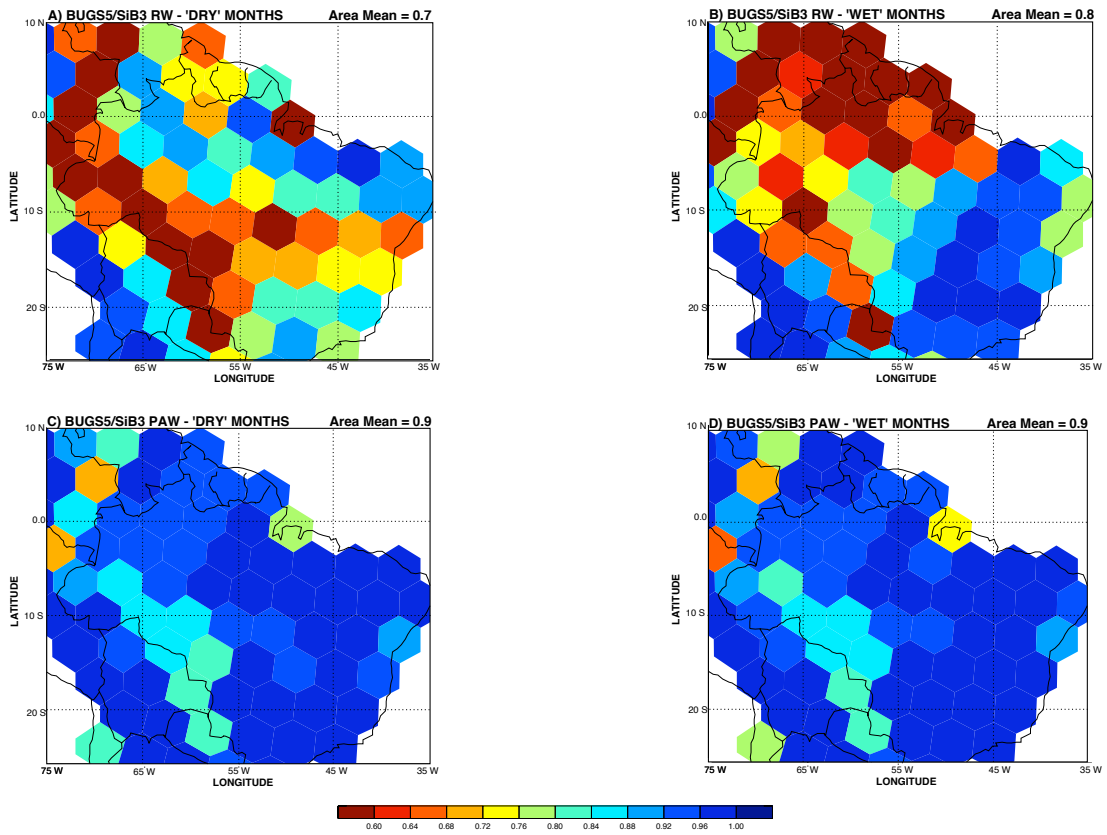

Figure 4.1 Soil moisture stress factor for the two versions of the model during dry and wet months. When the stress factor is 1, the vegetation is not stressed by deficits in soil moisture. Lower values of the stress factor impose more stress.

Dry season transpiration results in increased latent heat and decreased sensible heat fluxes in SiB3 PAW. Figures 4.2 and 4.3 show the difference between wet and dry season fluxes in the models. The latent heat flux is higher in SiB3 PAW throughout most of the basin during both seasons. The strongest differences are found along the western edge of the Amazon basin during the dry season and in the northern Amazon during the rainy season. These are areas where the soil moisture stress was greatly reduced in SiB3 PAW (Figure 4.1). Therefore, even though there is not a large difference in precipitation between the models in this region (Figure 4.8), the vegetation is less stressed by limited soil moisture.

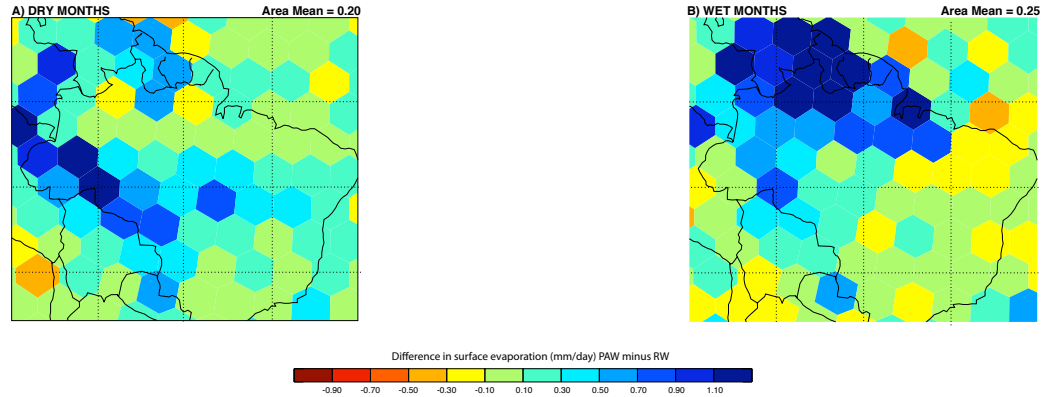

Figure 4.2 The differences in latent heat flux between the two models during the dry (a) and wet (b) months. Positive values mean that latent heat flux is stronger from SiB3 PAW. Latent heat has been converted to an evaporation rate from the surface.

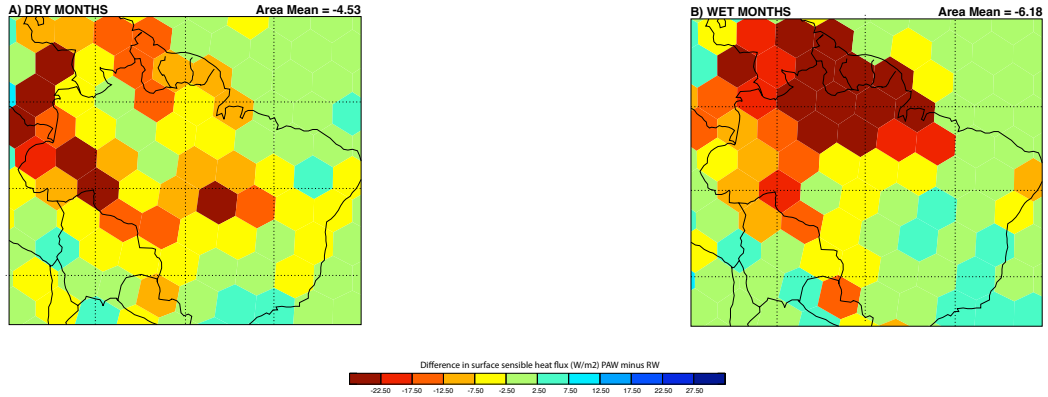

Figure 4.3 As in Figure 4.2 but for the sensible heat flux.

The decreased Bowen ratio (the ratio of sensible to latent heat) results in cooler temperatures in both seasons in SiB3 PAW (Figure 4.4). Despite more frequent cloud cover, southern Brazil is warmer during the wet season of both models due to increased solar radiation during the austral summer.

The increased latent heat also increases surface specific humidity (Figure 4.5). Compared to NCEP2 Reanalysis, SiB3 PAW does a better job of capturing the wet months' maximum in the central basin, but in general overestimates surface specific humidity.

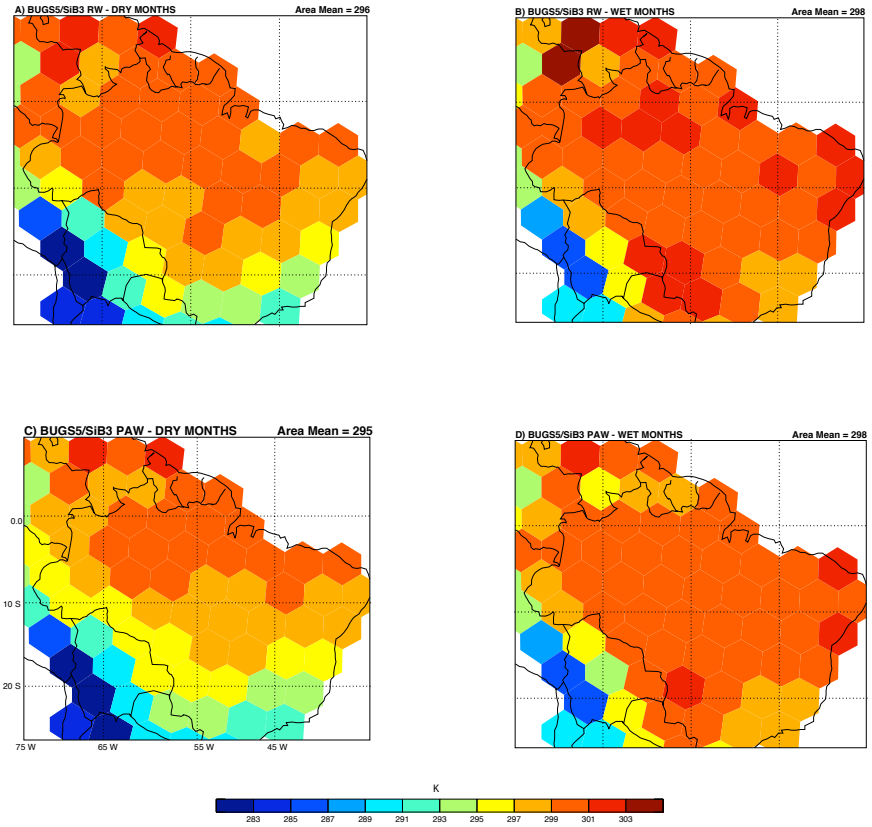

Figure 4.4 Air temperature within the canopy air space from BUGS5/SiB3 during wet and dry months. Units are Kelvin. Blues indicate cool temperatures and reds indicate warm temperatures.

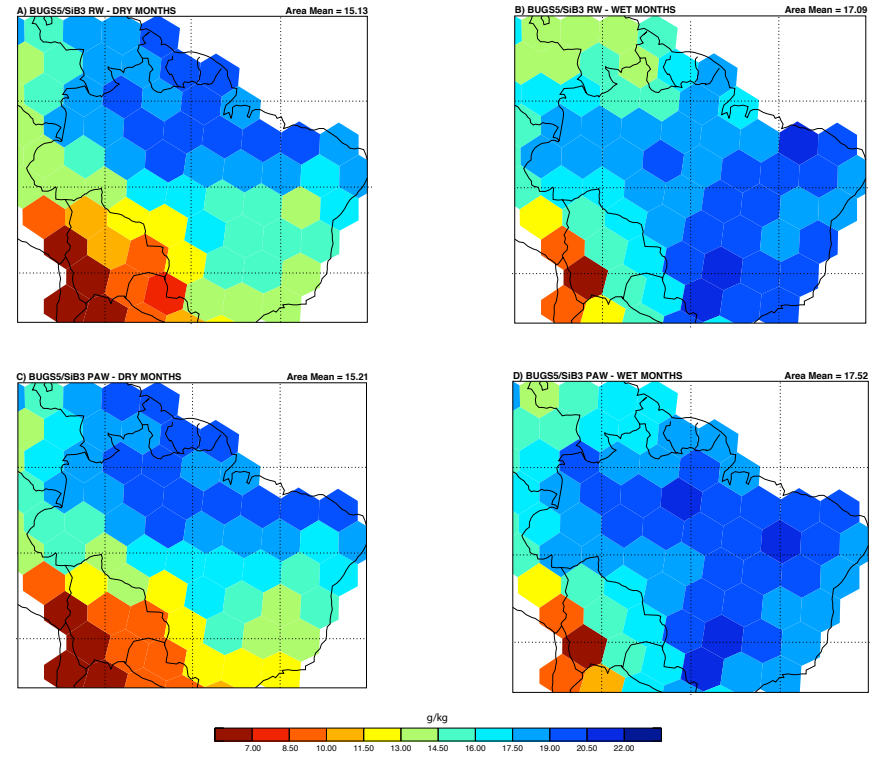

Figure 4.5 Specific humidity within the canopy air space from BUGS5/SiB3 during wet and dry months. Units are g/kg. Blues indicate more moisture.

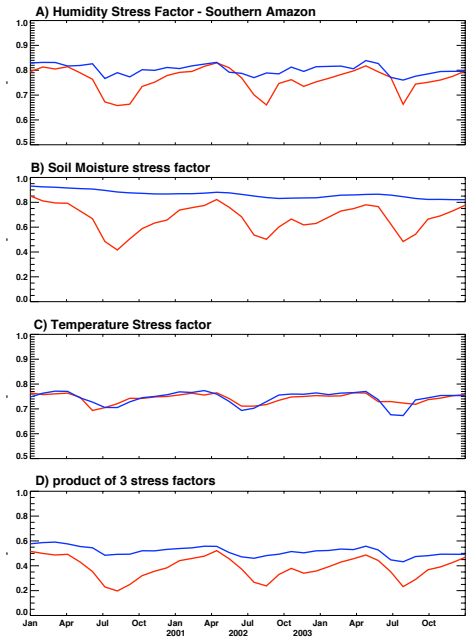

Figure 4.6 Simulated stress factors in the models in the southern Amazon. A value of 1 means the vegetation is unstressed. The three stresses (humidity, soil moisture, and temperature) are combined into one stress factor which modulates carbon assimilation and water loss through stomatal conductance.

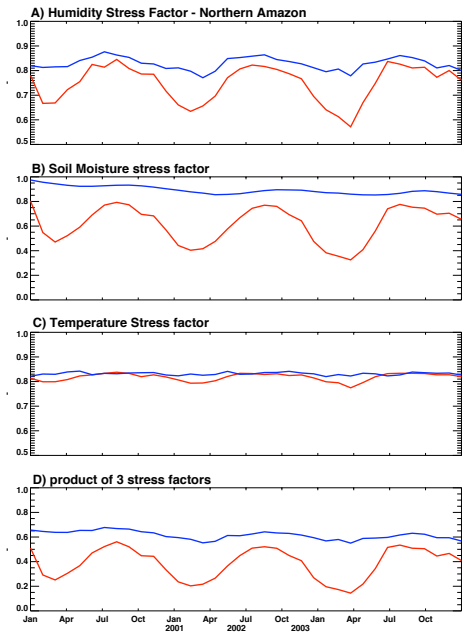

SiB3 RW SiB3 PAW

Figure 4.7 As in Figure 4.6 but for the northern Amazon.

The generally lower Bowen ratio in SiB3 PAW feeds back to reduce other stresses experienced by the vegetation. The seasonal cycle of the three stresses predicted by SiB is plotted in Figures 4.6 and 4.7 (for the southern and northern Amazon regions, respectively). In both regions, the total stress is reduced throughout the simulation period in SiB3 PAW (recall that lower stress corresponds to a higher stress factor). The difference is greatest during each region's dry season. It is particularly large in the northern Amazon where the difference in soil moisture stress is the strongest. Temperature stress is not strongly affected, but the humidity stress is decreased due to the increased evaporation.

4.2 EFFECTS ON METEOROLOGY

Figure 4.8 shows monthly composites of rainfall produced by SiB3 RW and SiB3 PAW. The changes in precipitation are from a combination of the changed fluxes of heat and moisture at the surface and changes in atmospheric circulation (discussed later). The model captures the movement of peak rainfall from north to south, but it does not place the maximum rain rates in the correct locations. In the dry season, the peak rainfall tends to fall along the coast and slightly to the east of the observed peak. The extension of rainfall along the coast is more pronounced in SiB3 PAW.

During the rainy season, GPCP shows maximum rainfall in the center of the basin. However, in the models the peak occurs along the southeastern coast. The rainy season pattern is somewhat similar to NCEP's rainfall, but there is too much precipitation

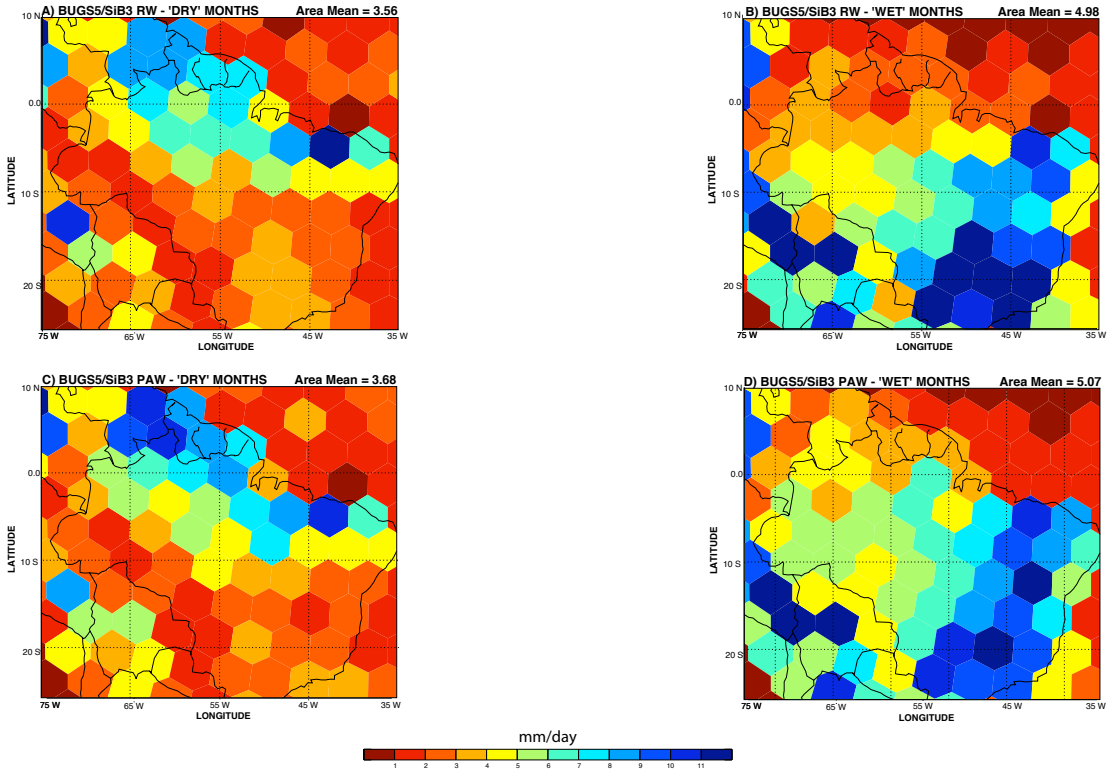

Figure 4.8 Monthly mean composites of rainfall from the two versions of the model during wet and dry months.

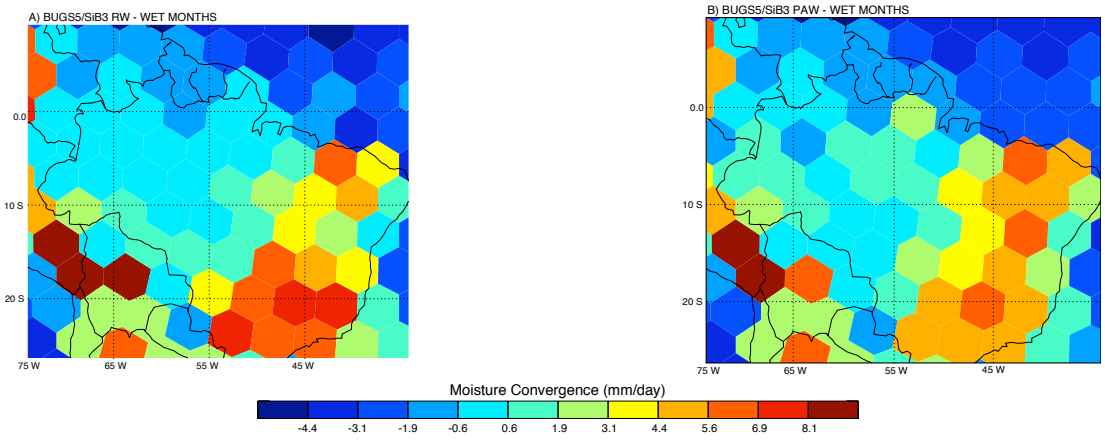

Figure 4.9 Moisture convergence during wet months in the model.

along the southeastern coast of Brazil. This displacement of wet season precipitation has occurred in previous versions of BUGS and is mostly a result of friction in the lowest level of the model (Don Dazlich, personal communication). Because the entire mixed layer is treated as one level, friction at the surface affects the entire layer. In the Amazon, where the roughness length is high, PBL winds are much lower than in the grasslands of southeastern Brazil. Therefore, low-level convergence of winds occurs more in the latter region. This affects total column convergence, as shown in Figure 4.9.

Despite this problem, SiB3 PAW seems to better capture the meridional gradient in rainfall near the equator. Also, precipitation along the southeastern coast of Brazil is decreased in SiB3 PAW, which is more in line with observations. This is an interesting result because this region is dominated by savannah. Therefore, it is treated similarly in both models. Clearly, changes in the Amazon rainforest have an effect on neighboring regions.

4.3 SEASONALITY OF THE HYDROLOGIC CYCLE IN THE NORTHERN AND SOUTHERN AMAZON

These comparisons show that simple changes in how the vegetation accesses soil moisture can change the surface conditions and precipitation. The next step is to examine the effect on the atmospheric hydrologic cycle, which is shown in Figures 4.10 and 4.11. The hydrologic cycle represents the balance between storage in the atmosphere and soil column with fluxes within and between the atmosphere and soil. The atmospheric portion of the budget is:

$$\frac{d(PW)}{dt} = LE + \int_{p\_pbl}^{p\_top} \mathbf{V} \bullet \nabla q \frac{dp}{g} - P \tag{3}$$

where PW is column-integrated precipitable water, LE is the surface evaporation, the vertical integral of $\boldsymbol{V} \cdot \nabla q$ represents regional moisture convergence, and P is precipitation.

The surface moisture budget can be computed as:

$$\frac{d(SM)}{dt} = P - R - LE \tag{4}$$

where SM is the soil moisture and R is runoff. Although BUGS5 tracks moisture in the atmosphere from grid cell to grid cell, SiB calculates runoff for each grid cell but it does not affect soil moisture in the adjoining grid cells.

By combining these two budgets, we obtain the total moisture budget for the region:

$$\frac{d(PW)}{dt} + \frac{d(SM)}{dt} = \int_{p\_pbl}^{p\_top} \mathbf{V} \bullet \nabla q \frac{dp}{g} - R \tag{5}$$

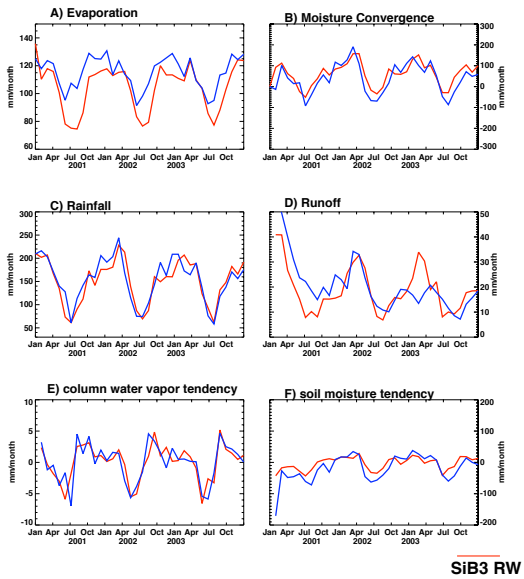

Figure 4.10 Components of the southern Amazon moisture budget (5°S to 15°S and 45° to 75°W), considering only land points with dominantly broadleaf evergreen vegetation.

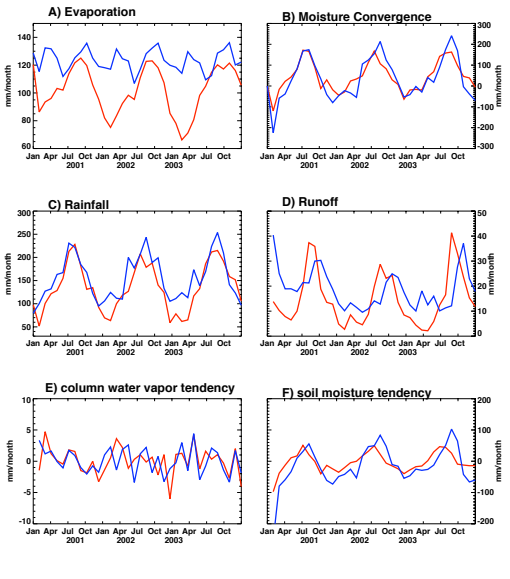

Figure 4.11 As in Figure 4.10 but for the nouthern Amazon (10°N to 5°S, 45° to 75°W).

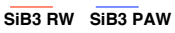

Figure 4.10 and 4.11 show the area-averaged seasonal cycles for the southern and northern Amazon regions, respectively, of evaporation (a), moisture convergence (b), precipitation (c), and runoff (d), as well as the monthly change in column precipitable water (e) and soil moisture (f).

In the northern Amazon, the rainy season occurs during the Northern Hemisphere summer. In SiB3 PAW, the rainfall is stronger in almost every month. This difference is maximized during the dry season of 2002-2003, when SiB3 PAW produces about 50 mm/ month more rainfall. The seasonal cycle of rainfall is closely linked to that of moisture convergence. During the rainy season, moisture is converging into the northern Amazon, and during the dry season there is moisture divergence.

Despite the seasonal cycles in moisture convergence and rainfall, the evaporation in SiB3 PAW does not show similar seasonality. In SiB3 RW, evaporation is limited by

the amount of rainfall, resulting in a pronounced seasonal cycle. However, in SiB3 PAW, there are two peaks each year - one in the mid to late rainy season and another towards the end of the dry season.

This sustained surface evaporation through the dry season allows for stronger moisture divergence and precipitation. The surface evaporation utilizes the soil moisture, causing it to decrease by as much as 70 mm/month. During the rainy season, evaporation is of similar magnitude, but there is strong moisture convergence and precipitation. Excess water is stored in the soil moisture, thereby replenishing what was lost during the dry season. In general, we see that by accessing deep soil moisture, the northern Amazon is able to be a source of moisture to surrounding regions even during periods of relatively low rainfall.

The seasonal cycle of rainfall is reversed in the southern Amazon (Figure 3.10). The rainy season occurs during the austral summer. The difference in precipitation between the models is not as distinct in the southern Amazon. However, the surface evaporation is different. In this region, both models show a seasonal cycle in evaporation, although evaporation is stronger in SiB3 PAW during both seasons. Also, in this version of the model, evaporation begins to increase in the middle of the dry season, whereas in SiB3 RW evaporation does not increase until the end of the dry season. The evaporated water is supplied by the soil column, and once in the atmosphere it is fluxed out of the region. Therefore, similar to the northern Amazon, the southern Amazon is a moisture source to surrounding regions during the end of its dry season. However, in contrast to

the northern Amazon, dry season precipitation is not strongly influenced by sustained surface evaporation.

Overall, the hydrologic cycle is more active in SiB3 PAW than in SiB3 RW. These seasonal and regional differences in the hydrologic cycle bring up a few questions that deserve further investigation - 1. Is dry and wet season precipitation fueled more by local moisture recycling or by moisture fluxes into the region? 2. What are the sources of the moisture fluxes? 3. What are the effects of increased dry season evaporation on the tropical circulation? The following three sections will deal with these questions.

4.4 AMAZON MOISTURE RECYCLING

Recall from Section 2.3 that the recycling ratio is essentially a ratio of local evaporation to precipitation plus horizontal moisture flux (Equation 1). We use a length scale of 2750 km to calculate the recycling ratio during wet and dry months in both models. The results are shown in Figures 4.12, 4.13, and 4.14. At most, between 25 and 30% of both regions' rainfall comes from local evaporation. In both regions of the Amazon, the recycling ratio is greater using SiB3 PAW in almost every month of the three-year simulation (Figure 4.13a and 4.14a). In other words, more rainfall is originating from local evaporation in SiB3 PAW. Although ρ is increased in SiB3 PAW, it is still less than observations by Trenberth (1999) and Eltahir and Bras (1994). The difference between the models is particularly evident in the central basin during both seasons, and in the northern basin during the wet months (Figure 4.12).

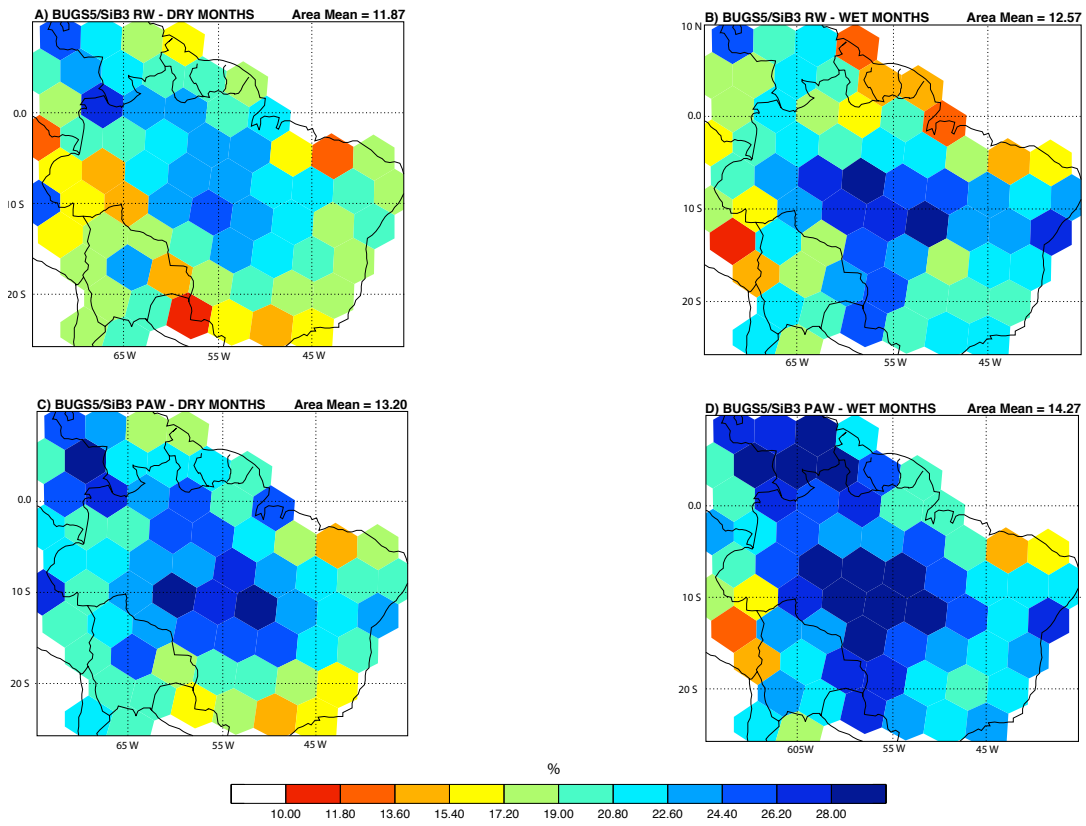

Figure 4.11 Recycling ratio from Trenberth (1999) for SiB3 RW and SiB3 PAW during dry and wet months. L=2750 km.

On a local basis, the strongest increases in ρ are in the south-central Amazon - where precipitation did not greatly increase but evaporation did (Figure 4.12). The location of the regional maximum produced by SiB3 PAW is in line with observations, but its magnitude is a little low. Also, the magnitude of moisture flux is higher in SiB3 RW (Figure 4.15). Therefore, due to the changes in SiB3 PAW, southern Amazon precipitation is fueled more by local evaporation and less by moisture flux. This change makes the recycling ratio closer to its observed values.

On the other hand, the northern Amazon wet months maximum produced by SiB3 PAW overestimates the importance of local evaporation (Figure 4.12 c & d). In observations, transport from the Caribbean and ITCZ supply most of the moisture for

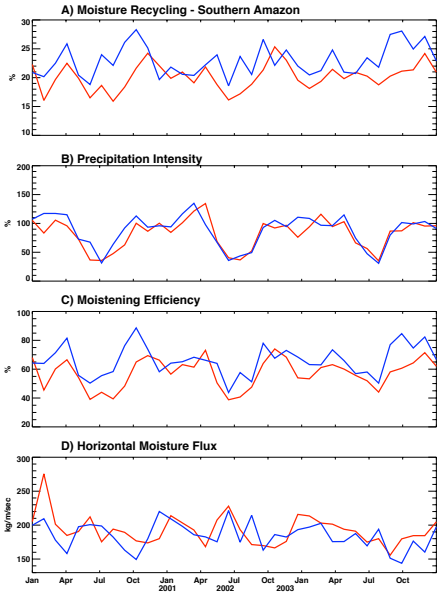

Figure 4.13 Recycling ratio (a), precipitation intensity (b), moistening efficiency (c), and horizontal moisture flux (d) in the Southern Amazon (5° to 15°S, 45° to 75°W), considering only land points with dominantly broadleaf evergreen vegetation.

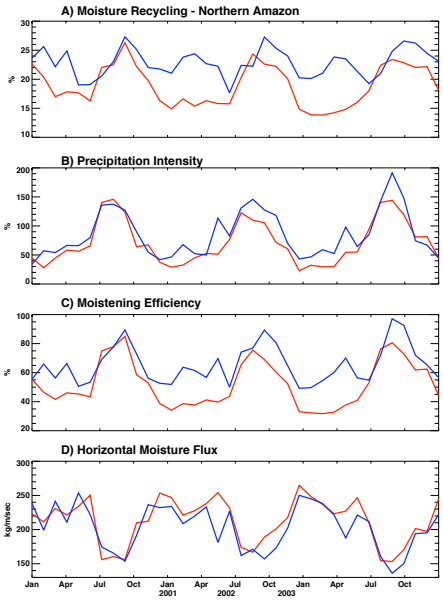

Figure 4.14 As in Figure 4.13 but for Northern Amazon (10°N to 5°S, 45° to 75°W).

rainfall in this region (Eltahir and Bras, 1994; Trenberth 1999). Also, the precipitation intensity, which is essentially a ratio of precipitation to horizontal moisture flux, is greater than 100% during the northern Amazon rainy season (Figure 4.14b).

According to Equation 1, the reason for the overestimation of the recycling ratio in the northern Amazon could be overestimated evaporation, or underestimated precipitation and/or moisture flux. Recall that during the wet months, precipitation is actually decreased in the northernmost region of the Amazon (Figure 4.8). In SiB3 PAW, evaporation is greatly increased in this region (Figure 4.2) and moisture flux is slightly lower (Figure 4.15). It is likely that a combination of these two factors leads to the overestimated recycling ratio in the northern Amazon.

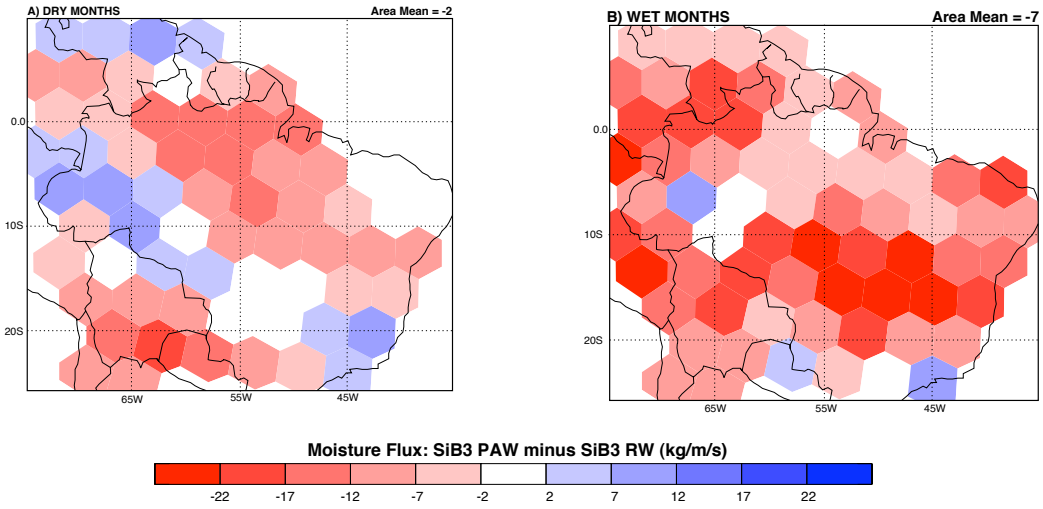

Figure 4.15 The difference in horizontal moisture flux between the two models during dry (a) and wet (b) months. Blues indicate that moisture flux is stronger in SiB3 PAW, and reds indicate that moisture flux is stronger in SiB3 RW.

4.5 SOURCES OF MOISTURE

The moisture flux, *F*, as shown in Equation 2 (section 3), is the vertically integrated amount of moisture being moved through each grid cell. *F* is larger in SiB3 RW in both seasons. Therefore, the changes in how the plants access soil moisture has affected large-scale circulation patterns and not just the local evaporation.

Although this is an interesting result we also want to know where the moisture is coming from. Vectorized, column-integrated moisture flux is shown in Figure 4.16. The red arrows are from SiB3 PAW, and the black arrows are from SiB3 RW. During the dry months, there is strong transport of moisture from the Atlantic into the northern Amazon. The strong moisture flux extends to 10°S and could explain the overestimation of precipitation along the northeastern Brazilian coast and south of the equator in the models. Above the savannahs of southeastern Brazil, there is weak anticyclonic flow,

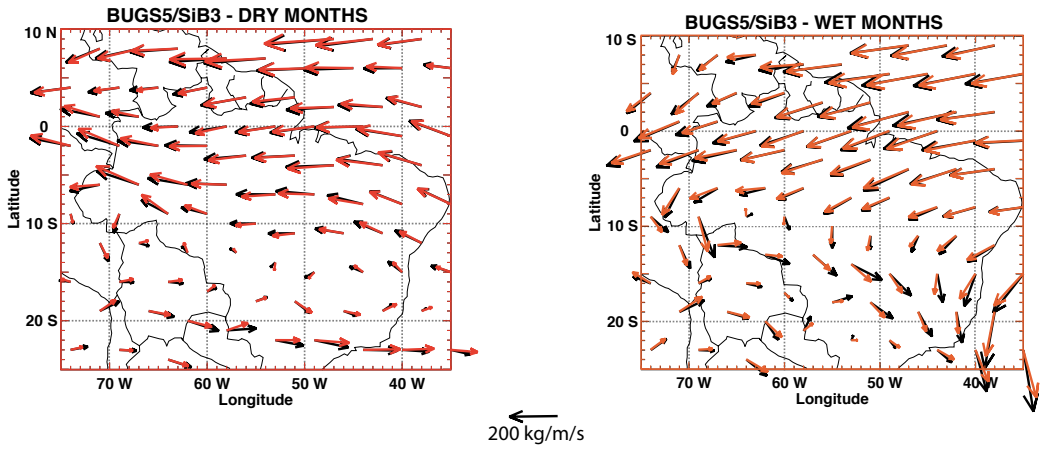

Figure 4.16 Model-produced moisture flux. The arrows represent the horizontal movement of water integrated throughout the atmospheric column. The red arrows are from SiB3 PAW, and the black arrows are from SiB3 RW.

which is slightly stronger in SiB3 RW. This circulation pattern is best seen in the 700 mb geopotential heights (Figure 4.17). In south central Brazil, the 700 mb isobar is elevated in SiB3 RW, coinciding with a region of increased sensible heat flux (Figure 4.3).

During wet months, strong moisture fluxes occur along the northeastern coast of Brazil, although there is not heavy rainfall in these regions. The flow of moisture goes from the coastal regions and across the Amazon, converging in the southern Amazon and in southeastern Brazil. This indicates that precipitation in this region is partially influenced by moisture fluxes within the rainforest, and is another way to look at the importance of Amazon surface evaporation to regional precipitation.

SiB3 PAW produces weaker moisture flux (and weaker precipitation) than SiB3 RW in southeastern Brazil. In southeastern Brazil, the Bowen ratio is higher in SiB3 PAW (Figures 4.2 and 4.3). This region is dominated by savannah ("cerrado") and short vegetation (Figure 3.3). As mentioned at the beginning of Chapter 4, moisture convergence is stronger in southeastern Brazil in BUGS. The convergence is slightly stronger in SiB3 RW (Figure 4.9). There is a positive feedback at play in this region. The

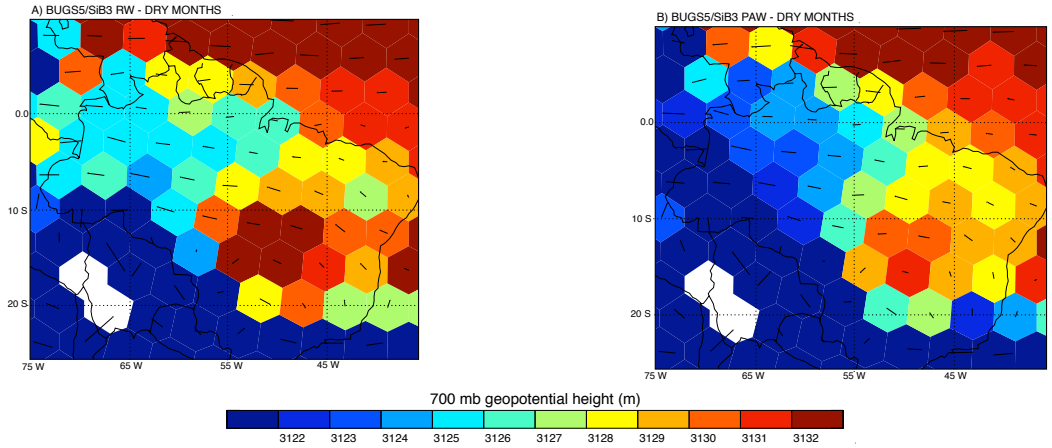

Figure 4.17 Modeled 700 mb geopotential height field during the dry months

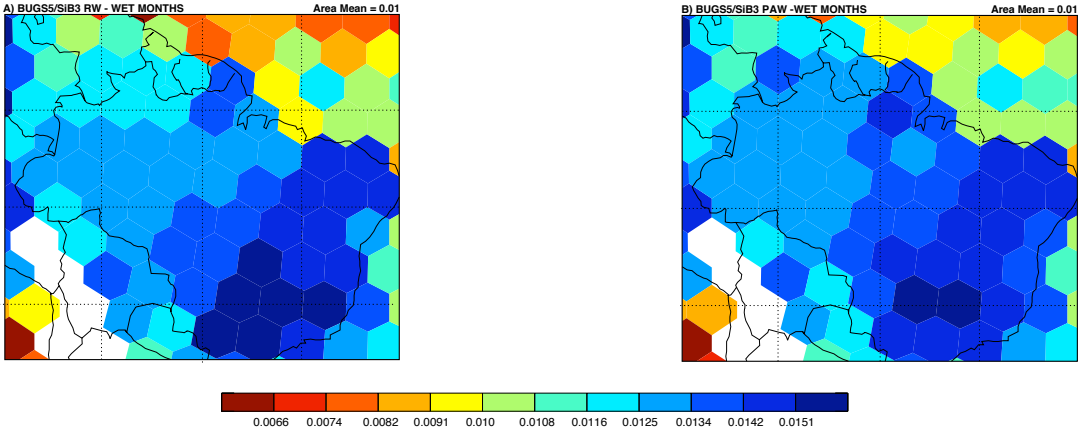

Figure 4.18 Specific humidity (kg/kg) of the modeled atmosphere at 850 mb during the wet months.

increased precipitation in SiB3 RW leads to more moisture on the surface (ie: puddles), which is evaporated and again made available for precipitation (figures not shown). As a result, in SiB3 PAW, moisture fluxes are decreased in this region and the 850 mb specific humidity is lower (Figure 4.18).

4.6 DYNAMICAL FORCING OF AMAZONIAN PRECIPITATION

Now that we have an understanding of the impacts of sustained dry season transpiration on meteorology and the hydrologic cycle, we can examine if there is also an effect on the dynamical qualities of the Amazonian wet season. Average circulation patterns from the three January's of the model runs are shown in Figure 4.19. The Bolivian high shows up in both geopotential height fields and as anticyclonic flow in the horizontal winds, although the center of the circulating winds is slightly displaced from the center of high pressure. The location of the Bolivian high is similar to that found by Lenters and Cook (1997) in the NASA/DAO observations.

In SiB3 RW, there is a secondary high located near the equator and 80°W. Winds are weak above the central basin, and then begin to flow toward the northeast above southeastern Brazil. Although there is a trough east of the Bolivian high, it is located farther east than the observed trough and the Nordeste low is not present.

In SiB3 PAW, circulatory patterns at 200 mb agree relatively well with the observations. Anticyclonic flow around the Bolivian high is better defined than in SiB3 RW. Also, the Nordeste low shows up clearly in this simulation. Therefore, the surface processes have a strong effect on the upper atmospheric circulation, and it is encouraging that the change is in the direction of better agreement with observations.

Figure 4.19 c and d show the outgoing longwave radiation (OLR) from the models. Compared to observations by Horel et al. (1989), the region of strong convection is displaced to the south in both versions of the model and both models seem to

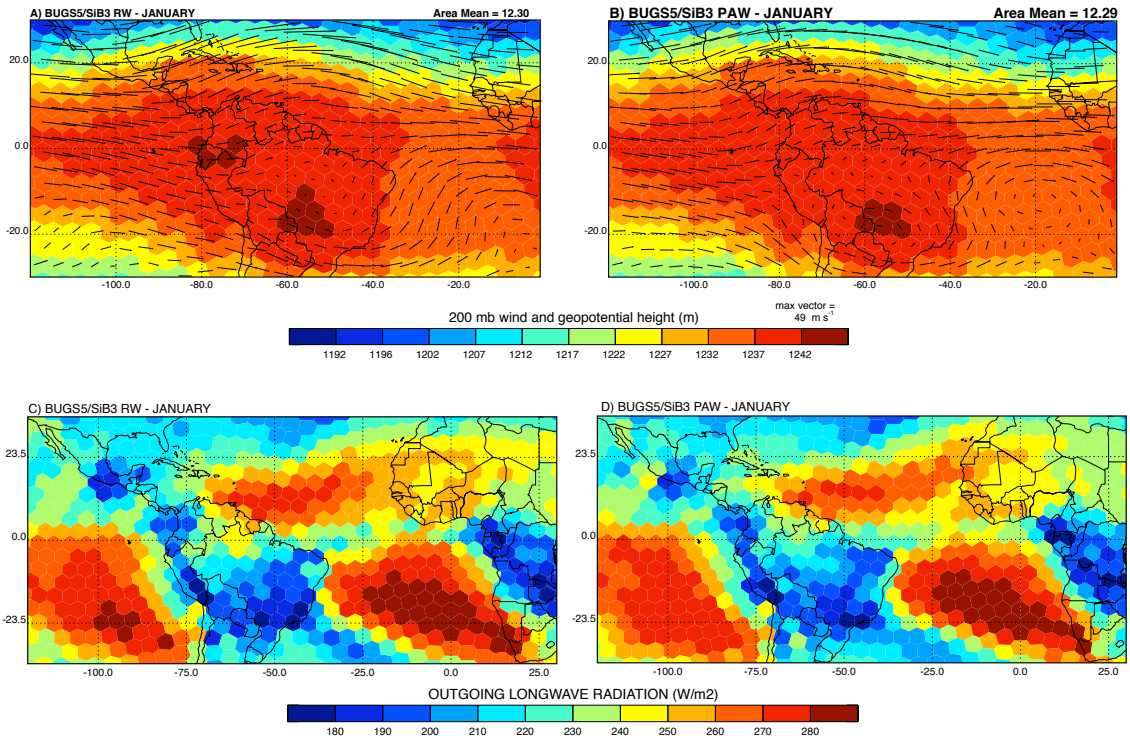

Figure 4.19 Modeled 200 mb circulation and geopotential heights (a,b) and OLR (c,d) over the region of Central and South America for January. The maximum wind vector is 49 m/s.

overestimate convection near Panama and southern Mexico. However, the northern boundary of convection is more in line with observations in SiB3 PAW.

As explained in the introduction, several studies (Silva Dias et al. 1983; Lenters and Cook 1997) have suggested that the Bolivian high is a result of latent heating in the atmosphere due to austral summer precipitation. The high is typically located to the southwest of the atmospheric heating maximum. Therefore, we examine mid-tropospheric (400 mb) heating due to moist convective processes and stratiform clouds. Above the Amazon, the former plays a larger role. This heating is shown in Figure 4.20a and b, and the difference between SiB3 RW and SiB3 PAW is shown in Figure 4.20c.

The maximum heating occurs over the savannahs of eastern Brazil. This is consistent with the maximized precipitation in these regions in the models. Within the

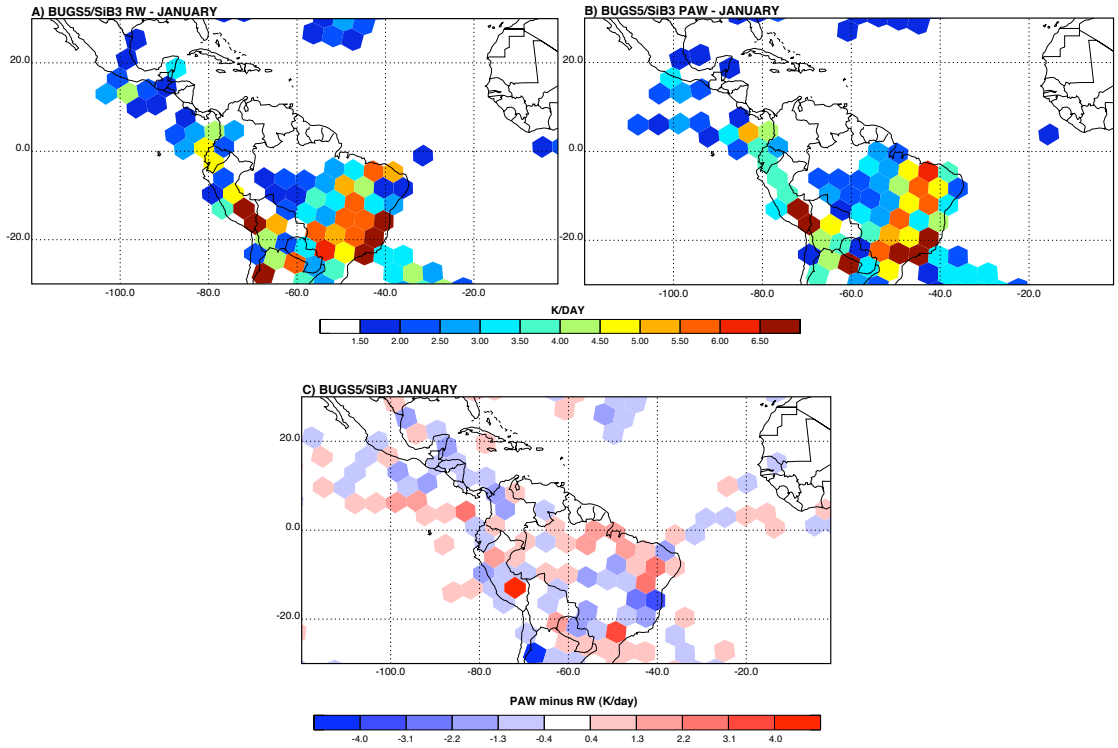

Figure 4.20 Sum of modeled temperature tendency at 400 mb due to moist convective processes and stratiform clouds (a,b). Values less than 1.5 K/day are not shown. C)The difference between SiB3 PAW and SiB3 RW 400 mb temperature tendencies. Blues indicate that heating is stronger in SiB3 RW and reds indicate that heating is stronger in SiB3 PAW.

region of maximum heating, SiB3 RW heating is greater to the southwest and SiB3 PAW heating is greater to the northeast. Lenters and Cook (1997) found that the position of the Bolivian high is most strongly influenced by condensation above the Amazon basin. Indeed, the atmospheric heating is generally greater above the Amazon forest in SiB3 PAW, where we expect the maximum heating to be based on NCEP2 and GPCP observations.

Therefore, a possible explanation for the difference in 200 mb circulation between the models is this shift in location of maximized atmospheric heating. The SiB3 PAW model more closely matches observations of precipitation in the southern Amazon and southeastern Brazil. The changes in location of maximized atmospheric heating due to

condensation of precipitation is therefore shifted, leading to a more realistic placement of the Brazilian high.

Lenters and Cook (1997) also found that the cyclonic circulation around the Nordeste low is strongly influenced by precipitation in the Amazon, SACZ, and tropical Africa. Precipitation in the SACZ is stronger in SiB3 RW, and in tropical Africa it is generally stronger in SiB3 PAW. Broadleaf evergreen vegetation dominates in parts of central Africa, therefore it is not surprising that SiB3 PAW produces stronger precipitation there. The increased precipitation produces more realistic cyclonic flow in the subtropical south Atlantic.

4.7 EFFECTS ON GLOBAL HEAT AND MOISTURE

Although this study focuses on changes within tropical South America, the changes in SiB3 PAW apply in other regions where broadleaf evergreen trees are the dominant vegetation type. These regions include equatorial Africa, Indonesia, Myanmar, Papau New Guinea, Malaysia, and parts of Central America. Therefore, the changes discussed in this section result from less soil moisture stress throughout the tropics. As shown in Figure 4.21, sensible heat flux (a & b) is decreased and latent heat flux (evaporation - c & d) is increased throughout the regions with tropical forests. These results are consistent with what we found in the Amazonian region.

Changes in fluxes from the continents result in interesting differences in fluxes from the oceans. For example, in December, January, and February (DJF), sensible heat fluxes are strongly increased from the northern Gulf Stream, where warm ocean water

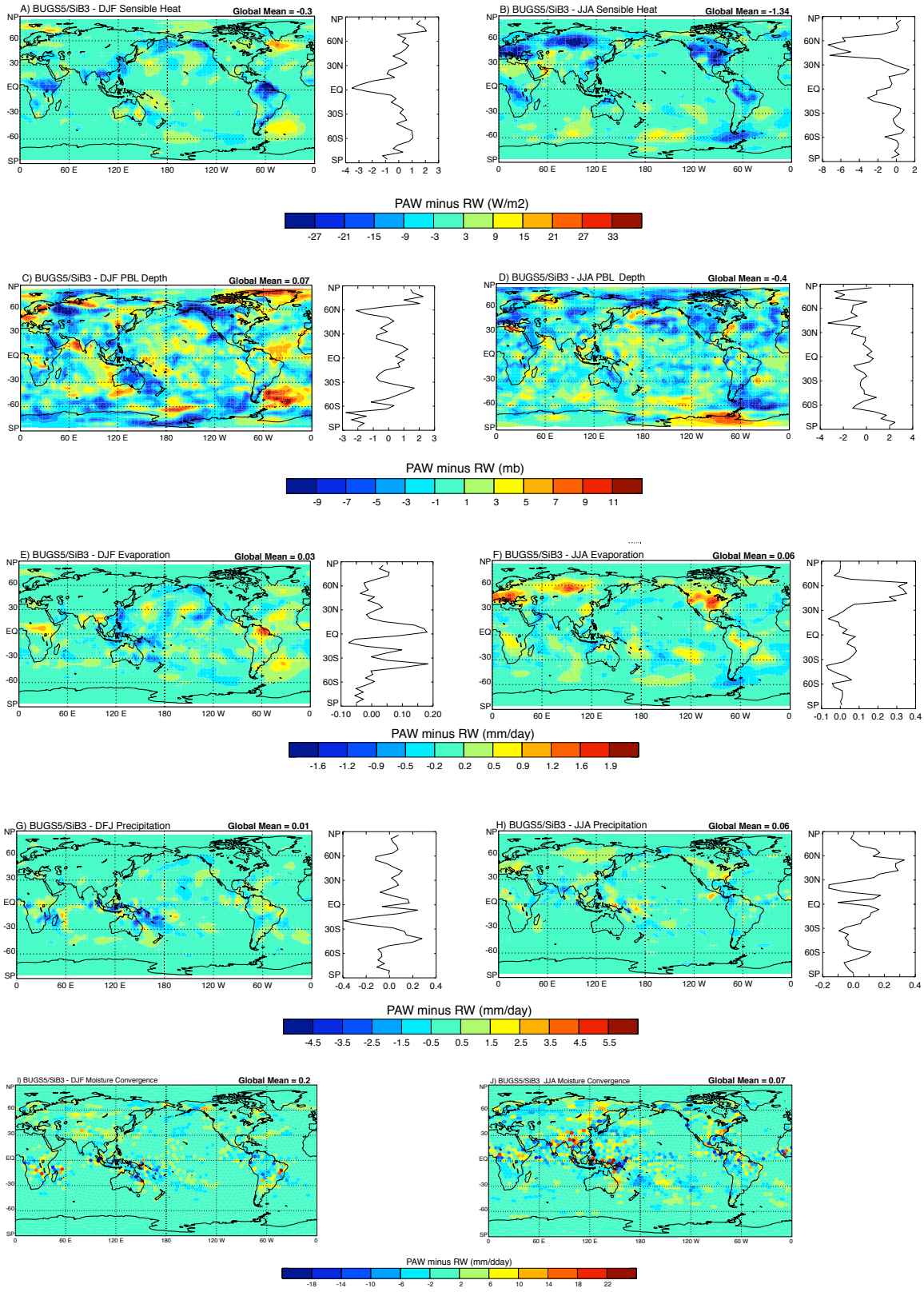

Figure 4.21 Comparison of SiB3 RW and SiB3 PAW for sensible heat flux, PBL depth, evaporation, precipitation, and moisture convergence for DJF and JJA. Positive values denote that SiB3 PAW values are greater than SiB3 RW.

fluxes heat into cool air. This change occurs due to a combination of small increases in ocean temperature (less than 1 K) and large decreases in surface air temperatures over the North American continent. A similar change occurs in the South Atlantic ocean off the southeastern tip of Argentina. Therefore, the ability of tropical forests to access deep soil moisture affects vegetation and climate in the mid and high latitudes, which leads to changes in ocean surface conditions downwind. The changes in sensible heat flux also result in shallower boundary layers over most continental regions. The boundary layer is deeper over several ocean regions where the sensible heat flux is greater in SIB3 PAW.

Surface evaporation increases in SiB3 PAW in the same regions that sensible heat decreases. In fact, it is the increased latent heat flux that causes the decreased heat flux. An interesting effect is decreased evaporation and precipitation in the western Pacific warm pool region in DJF. There is increased moisture convergence to the west of this region, but decreased convergence east of Papau New Guinea. Therefore, the increased evaporation from the tropical forests encourages local moisture convergence and decreases the gradient in water vapor between the atmosphere and ocean to the west, thereby decreasing the latent heat flux. Another area that experiences a large change between the models is in the Northern Hemisphere continental midlatitudes in June, July, and August (JJA). The precipitation is increased due to more surface evaporation and moisture convergence in SiB3 PAW.

5. DISCUSSION

The results of this study make a compelling argument for allowing plants to access deep soil moisture in a realistic manner in land surface models. This can be done through explicit inclusion of hydraulic redistribution (HR), as in Lee et al. (2005), or through adjustments of soil depth, rooting profiles, and stress calculations, as in this study and Baker et al. (2008). Doing so enables sustained dry season evapotranspiration and forest productivity, which is what we see in observations (Huete et al. 2006; Saleska et al. 2003; Oliveira et al. 2005). On the other hand, not including these parameterizations could lead to some of the catastrophic results discussed in the introduction. This study has shown that changes in surface fluxes affect the regional climate through precipitation and the circulation. Therefore, incorrectly simulating the surface fluxes could lead to unrealistic results in the climate. However, due to the short time period of the model runs (three years), it is not possible to assess from this study the climatic effects of extreme, long-term drought in the Amazon. This is an area warranting further investigation.

Below is a summary of the changes we found by allowing soil layers with high water content but low root density to make a large contribution to the plants evaporative demands.

- In SiB3 PAW, soil moisture stress is removed throughout much of the Amazon during both the wet and dry seasons.
- Dry season evapotranspiration is increased and sensible heat flux is decreased.
- Humidity stress is also decreased in SiB3 PAW.
- The surface is cooler and more moist in SiB3 PAW.
- Basin-averaged precipitation is stronger in SiB3 PAW. The largest increases occur in the northern Amazon during the dry months of May through August and in the central basin during the the wet months of November through March. Although both versions of the model overestimate precipitation over the savannahs in southeastern Brazil during the wet months, the mismatch with observations is less in SiB3 PAW.
- SiB3 PAW generally has a stronger hydrologic cycle. For example, in both the northern and southern regions, stronger dry season evaporation fuels stronger moisture divergence and precipitation.
- SiB3 PAW's precipitation originates more from local evaporation and less from fluxes of moisture.
- As in calculations from observations (Trenberth, 1999; Eltahir and Bras, 1994), SiB3 PAW produces a maximum in the recycling ratio in the central Amazon basin. In this region, more than 28% of precipitation originates from local evaporation.
- In the northern region, SiB3 PAW overestimates the recycling ratio, due to a combination of strong evaporation and weak moisture flux.

- SiB3 PAW has weaker moisture flux, with the largest difference occurring above the grasslands in southeastern Brazil. In this region, SiB3 PAW produces less precipitation than SiB3 RW, resulting in greater sensible heat fluxes and higher atmospheric pressure, conditions which do not stimulate strong moisture transport.
- SiB3 PAW leads to stronger convection in the central Amazon, which means the atmospheric heating due to condensation of water vapor is greater in this region. This has an effect on the position and strength of the Bolivian high.
- SiB3 PAW does a much better job of simulating the closed Nordeste low and related trough, possibly due to differences in precipitation above the central Amazon, South Atlantic Convergence Zone, and tropical Africa between the models.

In summary, this study has shown two things. First, processes that occur at the surface have a strong effect on regional meteorology and the large-scale circulation. And second, by creating a more realistic representation of vegetation in the Amazon, the model simulates more realistic results in many ways.

While this study has answered many questions, it has also created the opportunity to further investigate others. One area we wish to improve in the model is the patterns of precipitation in the Amazon. BUGS has historically overestimated the strength of the ITCZ and SACZ (Don Dazlich, personal communication). Also, this model was ran on a relatively coarse grid, and we would like to run it at a higher resolution and perhaps use

observed (rather than climatological) SST's. This would allow topography (particularly the Andes) to play a more realistic role in Amazon moisture convergence. It would also permit a study of how the land-atmosphere interactions discussed in this paper react to El Nino and La Nina conditions. A study of the former is particularly pertinent because of predictions of El Nino-like conditions in the Amazon in the future (Oliveira et al. 2005; Cox et al. 2004).

In addition to the monthly output utilized in this study, we have hourly output at several sites throughout the Amazon coinciding with observation sites from the LBA campaign. It is beyond the scope of this study but of extreme interest to examine the length, timing, and intensity of the wet season at these sites. We would like to know if the model is correctly simulating these variables, and also if it is doing so for the right reasons. Fu et al. (2005) examined several meteorological conditions during the dry to wet season transition using ECMWF reanalysis and a similar study utilizing the point-by-point output would tell us a lot about land-atmosphere interactions' impact on the return of the rainy season in the Amazon. The implications of such a study are of great interest as humans continue to modify land cover in this region, and because wet season length has been shown to be a major factor in how much total precipitation falls each year.

Finally, SiB3 simulates exchanges of carbon between the land and atmosphere. Several recent observations imply that the rainforest is a source of carbon to the atmosphere during the dry season and a sink during the wet season. The changes in vegetation stress have surely had an effect on the land's carbon budget, which is something we would like to study in the future.

IV. CONCLUSIONS

In summary, two versions of the Simple Biosphere model coupled to the CSU GCM were compared. In SiB3 RW, plants extract water from the root zones with the most roots. The soil in this model was only 3.5 meters deep. In SiB3 PAW, plants were able to extract water from any layer that had roots - allowing the layers with high water content but lower root density make a large contribution to the plants evaporative demands. The SiB3 PAW soil was 10 meters deep.

We first examined the effects of deep roots and improved soil moisture stress representation on the surface fluxes and hydrologic cycle at a site in the central Amazon basin. SiB3 RW does not accurately simulate the seasonal cycles of heat and moisture fluxes. In SiB3 PAW, dry season evapotranspiration increases and sensible heat fluxes decrease, resulting in a closer match to observations. These changes cool and moisten the boundary layer, which in a real atmosphere would result in lowered surface pressures and a more conducive environment to moisture convergence and convection. SiB3 PAW also produces a more active hydrologic cycle on seasonal and diurnal time scales.

We next implemented SiB3 PAW and SiB3 RW in a full GCM in order to investigate interactions between the surface fluxes and large-scale circulation. The

changes in fluxes are similar to those in the single column model - namely increased dry season transpiration, decreased sensible heat flux.

In both the northern and southern Amazon, stronger dry season evaporation flues stronger moisture divergence and precipitation. The largest increases occur in the northern Amazon during the dry months of May through August and in the central basin during the the wet months of November through March. The stronger convection over the central Amazon result in stronger atmospheric heating and a more realistic simulation of the Bolivian high and Nordeste low, both important upper-tropospheric features of the Amazonian wet season.

In the savannahs in southeastern Brazil, SiB3 PAW produces less precipitation than SiB3 RW. This result brings precipitation in this region closer to observations and leads to greater sensible heat fluxes and higher atmospheric pressure. These conditions result in weaker regional moisture transport in SiB3 PAW, which feeds back to the original result of decreased precipitation. We also see affects of tropical forest soil moisture representations on global fields of heat and moisture fluxes, boundary layer depth, precipitation, and moisture convergence.

Our goal in this study was to investigate the effects soil moisture stress and root-zone dynamics on land-atmosphere interactions, and to determine how these interactions may or may not influence extreme drought. We have found that the root-zone representations in SiB3 PAW realistically simulate local fluxes of heat and moisture, particularly during the dry season. Compared to SiB3 RW, which simulates very little dry season evapotranspiration, the atmosphere in SiB3 PAW is more conducive to moisture

convergence and convection. Because plants are able to transpire during dry periods, hydrologic cycle is more active. It is unlikely that such an atmosphere would dry out completely, as has occurred in previous modeling studies.

V. BIBLIOGRAPHY

Arakawa, A. and W.H. Schubert, 1974: Interaction of a Cumulus Cloud Ensemble with the Large-Scale Environment, Part I. *Journal of Atmospheric Sciences*, **31(3)**, 674-701.

Baker, I.T., L. Prihodko, A.S. Denning, M. Goulden, S. Miller, H.R. da Rocha, 2008: Seasonal Drought Stress in the Amazon: Reconciling Models and Observations

Bala, C., K. Caldeira, A. Mirin, M. Wickett, and C. Delire, 2005: Multicentury changes to the global climate and carbon cycle: Results from a coupled climate and carbon cycle model. *J. Climate,* **18,** 4531-4544.

Betts, A.K., and M.J. Miller, 1986: A new convective adjustment scheme, II, Single column tests using GATE wave, BOMEX, ATEX, and arctic air-mass data sets, *Quarterly Journal of the Royal Meteorological Society,* **112**, 693-709.

Bonan, G.B., 1996. Land Surface Model (LSM version 1.0) for Ecological, Hydrological, and Atmospheric Studies. *National Center for Atmospheric Research Technical Report*.

Brando, P.M., D.C. Nepstad, E.A. Davidson, S.E. Trumbore, D. Ray, P. Camargo, 2008: Drought effects on litterfall, wood production and belowground carbon cycling in an Amazon forest: results of a throughfall reduction experiment. *Philosophical Transactions of the Royal Society - Biological Sciences*, **363(1498)**, 1939-1848.

Brown, M.E.**,** J. Pinzon and C.J. Tucker, 2004: New Vegetation Index Dataset Available to Monitor Global Change, *EOS Transactions*, **85**, 565.

Clapp, R.B. and G.M Hornberger, 1978: Empirical Equations for Some Soil Hydraulic Properties. *Water Resources Research*, **14(4)**, 601-604.

Collatz, G.J., J.T. Ball, C. Grivet, J.A. Berry, 1991: Physiological and Environmental Regulation of Stomatal Conductance, Photosynthesis and Transpiration: A Model that Includes a Laminar Boundary Layer. *Agricultural and Forest Meteorology*, **54**, 107-136.

Cox, P.M., R.A. Betts, C.D. Jones, S.A. Spall, and I.J. Totterdell, 2000: Acceleration of global warming due to carbon-cycle feedbacks in a coupled climate model. *Nature,* **408**, 184-187.

Cox, P.M., R.A. Betts, M. Collins, P.P. Harris, C. Huntingford, and C.D. Jones, 2004: Amazonian forest dieback under climate-carbon cycle projections for the 21st century. *Theor. Appl. Climatol.*, **78,** 137-156.

da Rocha, H.R. and Coauthors, 2004: Seasonality of water and heat fluxes over a tropical forest in eastern Amazonia. *Ecological Applications*, **14**, S22-S32.

Dai, Y. X. Zeng, R.E. Dickinson and Coauthors, 2003: The Common Land Model (CLM) version 1.0. *Bulletin of the American Meteorological Society*, **84**, 1013-1023.

Denning, A.S., G.J. Collatz, C. Zhang, D.A. Randall, J.A. Berry, P.J. Sellers, G.D. Colello, D.A. Dazlich, 1996: Simulations of Terrestrial Carbon Metabolism and Atmospheric CO_2 in a General Circulation Model. Part I: Surface Carbon Fluxes. *Tellus*, **48B**, 521-542.

Ding, P., and D. A. Randall, 1998: A Cumulus Parameterization with Multiple Cloud Base Levels. *Journal of Geophysical Research*, **103**, 11,341-11,354.

Farquhar, G.D., S. von Caemmerer, J.A. Berry, 1980: A Biochemical Model of Photosynthetic CO_2 Assimilation in Leaves of C3 Species. *Planta*, **149(1)**, 78-90.

Fiorino, M. (2000), "AMIP II sea surface temperature and sea ice concentration observations." http://www-pcmdi.llnl.gov/projects/amip/AMIP2EXPDSN/BCS_OBS/amip2_bcs.htm

Fowler, L. D., D. A. Randall, and S. A. Rutledge, 1996: Liquid and Ice Cloud Microphysics in the CSU General Circulation Model. Part 1: Model Description and Simulated Microphysical Processes. *J. Climate*, **9**, 489-529.

Fowler, L. D., and D. A. Randall, 2002: Interactions between cloud microphysics and cumulus convection in a general circulation model. *Journal of Atmospheric Sciences*, **59**, 3074-3098.

R. Fu, R. E. Dickinson, M. Chen, and H. Wang, 2001: How do tropical sea surface temperatures influence the seasonal distribution of precipitation in the equatorial Amazon?, *J. Climate,* **14,** 4003–4026.

Friedlingstein, P., and Coauthors, 2001: Positive feedback between future climate change and the carbon cycle. *Geophys. Res. Lett.*, **28**, 1543-1546.

Gabriel, P.M., P.T. Partain, G.L. Stephens, 2001: Parameterization of Atmospheric Radiative Transfer. Part II: Selection Rules. *Journal of the Atmospheric Sciences*, **58(22)**, 3411-3423.

Goulden, M.L., and Coauthors, 2004: Diel and seasonal patterns of tropical forest CO_2 exchange. *Ecological Applications*, **14**, S42-S54.

Hansen, M.C., R.S. Defries, J.R.G. Townshend, R. Sohlberg, 2000: Global Land Cover Classification at 1 km Spatial Resolution Using a Classification Tree Approach. *International Journal of Remote Sensing*, **21(6-7)**, 1331-1364.

Holben, B.N., 1986: Characteristic of maximum-value composite images for temporal AVHRR data, *International Journal of Remote Sensing*, **7**, 1435-1445.

Houghton, R.A., K.T. Lawrence, J.L. Hackler, S. Brown, 2001: The Spatial Distribution of Forest Biomass in the Brazilian Amazon: A Comparison of Estimates. *Global Change Biology*, **7**, 731-746.

Huete, A.R., K. Didan, Y.E. Shimabukuro, P. Ratana, S.R. Salexska, L.R. Hutyra, W. Yang, R.R. Nemani, R. Myneni, 2006: Amazon rainforests green-up with sunlight in dry season. *Geophys. Res. Lett.*, **33**, L06405.

Huffman, G.J., R.F. Adler, P. Arkin, A. Chang, R. Ferraro, A. Gruber, J. Janowiak, A. McNab, B. Rudolf, and U. Schneider, 1997, The Global Precipitation Climatology Project (GPCP) Combined Precipitation Dataset, Bulletin of the American Meteorology Society, **78 (1)**, 5-20.

Jipp, P.H., D.C. Nepstad, D.K. Cassel, and C. Reis de Carvalho, 1998: Deep soil moisture storage and transpiration in forests and pastures of seasonally-dry Amazonia. *Climatic Change*, **39**, 395-412.

Justice, C., et al. (1998), The Moderate Resolution Imaging Spectroradiometer (MODIS): Land remote sensing for global change research, *IEEE Trans. Geosci. Remote Sens.*, **36**, 1228-1249.

Li, W. and Fu, R., 2004: Transition of the Large-Scale Atmospheric and Land Surface Conditions from the Dry to the Wet Season over Amazonia as Diagnosed by the ECMWF Re-Analysis. *Journal of Climate*, 2637-2651.

Liebmann, B., and J. A. Marengo, 2001: Interannual variability of the rainy season and rainfall in the Brazilian Amazon Basin. *J. Climate,* **14**, 4308–4318.

Liu, Jun, 2004: Investigation of ecosystem drought stress and its impacts on carbon exchange at tropical forests. *M.S. Thesis*, CSU, Dept. of Atmospheric Science.

Los, S.O., C.O. Justice, and C.J. Tucker, 1994: A 1 by 1 global NDVI data set for climate studies calculated from the GIMMS continental NDVI data. *International Journal of Remote Sensing*, **15**, 3493-3518.

Los, S.O, N.H. Pollack, M.T. Parris, G.J. Collatz, C.J. Tucker, P.J. Sellers, C.M. Malmstrom, R.S. DeFries, L. Bounoua, D.A. Dazlich, 2000: A Global 9-year Biophysical Land Surface Dataset from NOAA AVHRR Data. *Journal of Hydrometeorology*, **1(2)**, 183-199.

Miller, S.D., M.L. Goulden, M.C. Menton, H.R. da Rocha, H.C. de Freitas, A.M.E.S. Figueira, C.A.D. de Sousa, 2004: Biometric and Micrometeorological Measurements of Tropical Forest Carbon Balance, *Ecological Applications*, **14(4)**, S114-S126.

Nepstad, D.C., C.R. de Carvlho, E.A. Davidson, P.H. Jipp, P.A. Lefebvre, G.H. Negreiros, E.D. da Silva, T.A. Stone, S.E. Trumbore, S. Viera, 1994: The role of deep roots in the hydrological and carbon cycles of Amazonian forests and pastures. *Nature*, **372**, 666-669.

Nepstad, D.C. and Coauthors, 2002: The effects of partial throughfall exclusion on canopy processes, aboveground production, and biogeochemistry of an Amazon forest. *Jour. of Geophys. Res.*, **107**, 53.

Nepstad, D.C. and Coauthors, 2004: Amazon drought and its implications for forest flammability and tree growth: a basin-wide analysis. *Global Change Biology*, **10**, 704-717.

Nepstad, D.C., I.M. Tohver, D. Ray, P. Moutinho, and G. Cardinot, 2007, Mortality of large trees and llanas following experimental drought in an Amazon forest, *Ecology*, **88(9)**, 2259-2269.

Oliveira, R.S., T.E. Dawson, S.S.O. Burgess, and D.C. Nepstad, 2005: Hydraulic redistribution in three Amazonian trees. *Oecologia*, **145**, 354-363.

Pan, D.-M., and D. A. Randall, 1998: A Cumulus Parameterization with a Prognostic Closure. *Quart. J. Roy. Met. Soc.*, **124**, 949-981.

Pinzon, J., M. E. Brown and C.J. Tucker, Satellite Time Series Correction of Orbital Drift Artifacts Using Empirical Mode Decomposition. In: *Applications of Empirical*

Mode Decomposition Chapter 10, Part II, Editor: Nordon Huang, 2006.

Rahman, A.F., D.A. Sims, V.D. Cordova, and B.Z. El-Masri (2005), Potential of MODIS EVI and surface temperature for directly estimating per-pixel ecosystem C fluxes, *Geophys. Res. Lett.*, **32**, L19404.

Randall, D. A., and D.M. Pan, 1993: Implementation of the Arakawa-Schubert Cumulus Parameterization with a Prognostic Closure. In *Cumulus Parameterization*, a Meteorological Monograph published by the American Meteorological Society, K. Emanuel and D. Raymond, Eds., pp. 137 - 144.

Randall, D. A., P. J. Sellers, J. A. Berry, D. A. Dazlich, C. Zhang, G. J. Collatz, A. S. Denning, S. O. Los, C. B. Field, I. Fung, C. O. Justice, C. J. Tucker, and L. Bounoua, 1996: A Revised Land-Surface Parameterization (SiB2) for Atmospheric GCMs. Part 3: The Greening of the CSU General Circulation Model. *J. Climate*, **9**, 738-763.

Randall. D.A. and D.G. Cripe, 1999: Alternative Methods for Specification of Observed Forcing in Single-Column Models and Cloud System Models. *Journal of Geophysical Research*, **104(D20)**, 24,527-24,545.

Randall, D. A., T. D. Ringler, R. P. Heikes, P. Jones, and J. Baumgardner, 2002: Climate modeling with spherical geodesic grids. *Computing in Science and Engr.*, **4**, 32-41.

Ringler, T. D., R. P. Heikes, and D. A. Randall, 2000: Modeling the atmospheric general circulation using a spherical geodesic grid: A new class of dynamical cores. *Mon. Wea. Rev.*, **128**, 2471-2490.

Saleska, S.R. and Coauthors, 2003: Carbon in Amazon forests: Unexpected seasonal fluxes and disturbance-induced losses. *Science*, **302**, 1554-1557.

Sellers, P.J., Y. Mintz, Y.C. Sud, A. Dalcher, 1986: A Simple Biosphere Model (SiB) for Use within General Circulation Models. *Journal of the Atmospheric Sciences*, **43(6)**, 505-531.

Sellers, P.J., J.A. Berry, G.J. Collatz, C.B. Field, and F.G. Hall, 1992: Canopy reflectance, photosynthesis, and transpiration III: A reanalysis using improved leaf models and a new canopy integration scheme. *Remote Sens. Environ.*, **42**, 187-216.

Sellers, P.J., D.A. Randall, G.J. Collatz, J.A. Berry, C.B. Field, D.A. Dazlich, C. Zhang, G.D. Colello, L. Bounoua, 1996a: A Revised Land Surface Parameterization (SiB2) for Atmospheric GCM's. Part I: Model Formulation. *Journal of Climate*, **9(4)**, 676-705.

Sellers, P.J., C.J. Tucker, G.J. Collatz, S.O. Los, C.O. Justice, D.A. Dazlich, D.A. Randall, 1996b: A Revised Land Surface Parameterization (SiB2) for Atmospheric GCM's. Part II: The Generation of Global Fields of Terrestrial Biophysical Parameters from Satellite Data. *Journal of Climate*, **9(4)**, 706-737.

Silver, W.L., Neff, J., McGroddy, M., Veldkamp, E., Keller, M., Cosme, R., 2000, Effects of Soil Temperature on Belowground Carbon and Nutrient Storage in a Lowland Amazonian Forest Ecosystem, *Ecosystems*, **3**, 193-209.

Stephens, G.L, P.M. Gabriel, and P.T. Partain, 2001: Parameterization of Atmospheric Radiative Transfer. Part I: Validity of Simple Models. *Journal of the Atmospheric Sciences*, **58(22)**, 3391-3409.

Taylor, K.E, Williamson, D., Zwiers, F., 2001, "AMIP II sea surface temperature and seas ice concentration boundary conditions," http://www-pcmdi.llnl.gov/projects/amip/amip2/AMIP2EXPDSN/BCS/amip2bcs.html.

Tempel, P., N.H. Batjes, and V.W.P. van Engelen, IGBP-DIS soil data set for pedotransfer function development. Working paper and Preprint 96/05, International Soil Reference and information Centre (ISRIC), Wageningen., 1996.

Trenberth, K.E., 1999: Atmospheric Moisture Recycling: Role of Advection and Local Evaporation. *Journal of Climate*, **12(5)**, 1368-1381.

Tucker C.J., Pinzon J.E., Brown M.E., Slayback D.A., Pak E.W., Mahoney R., Vermote E.F., and El Saleous N.. "An Extended AVHRR 8-km NDVI Data Set Compatible with MODIS and SPOT Vegetation NDVI Data", *International Journal of Remote Sensing*, 26 (20): 4485-4498, 2005.

Wang, H. and R. Fu, 2002, Cross-Equatorial Flow and Seasonal Cycle of Precipitation over South America, *Journal of Climate,* **15**, 1591-1608.